Table 5 Phase II study of amrubicin in relapsed case or refractory case with small lung cancer: Response

	Sensitive case	Refractory case	Total
No. of patients	44	16	60
CR	1	1	2
PR	22	7	29
SD	10	2	12
PD	11	6	17
Response rate (95% CI)	52% (37–68%)	50% (25–75%)	52% (38–65%)
Progression-free survival (95% CI)	4.2 months (3.6–5.3)	2.9 months (1.4–4.6)	3.9 months (3.4–4.6)
Median survival time (95% CI)	11.6 months (10.0–15.8)	10.3 months (4.8–∞)	11. months (10.0–13.2)
1-yr survival (95% CI)	45.5% (29.9–59.8)	40.3% (15.1–64.6)	44.1% (30.6–56.8)

∞: a symbol of infinite

Future directions

As noted above, little evidence has been published concerning the efficacy of amrubicin in the treatment of NSCLC or SCLC. Only amrubicin monotherapy has been investigated for NSCLC, and only combination therapy with cisplatin has been investigated for SCLC.

At present, platinum-based doublet chemotherapy is considered the standard treatment as 1st line chemotherapy for advanced NSCLC. Therefore, combination therapy with cisplatin in previously untreated patients with advanced NSCLC should be tested. Combination therapy with carboplatin, an analog of cisplatin that is often used instead of cisplatin because of its milder toxicity profile, should also be evaluated. However, in combination with carboplatin, it is necessary to note that hematologic toxicities overlap, and therefore studies should start from phase I to determine a recommended dosage. Combination therapies with paclitaxel, docetaxel, gemcitabine, vinorelbine, and CPT-11, novel anticancer agents that became available in the 1990s, should also be topics of investigation as non-platinum regimens. However, it is already known that anthracycline anticancer agents and taxane agents interact: for example, in combination therapy using paclitaxel plus doxorubicin, it has been reported that if paclitaxel is administered first, not only do the pharmacokinetics of doxorubicin change, but its toxicity is increased [18]. Because amrubicin is also an anthracycline agent, any investigation of combination therapy with a taxane agent in particular should involve a pharmacokinetics study. Recently, Masuda et al. conducted a combination phase I study of CPT-11 and amrubicin, which led to a recommended dosage of 60 mg/m^2 of CPT-11 on days 1 and 8, and 25 mg/m^2 of amrubicin, days 1–3 every 3 weeks, the lowest dosage levels that had been tested in their study because of adverse events, including strong myelotoxicity [19]. Regardless of whether or not it is combined with a platinum drug, it is necessary to clarify whether amrubicin can become a viable first line chemotherapy candidate for advanced NSCLC in the future.

Table 6 Responses of the "3rd generation drug" in sensitive relapse and refractory disease[a]

	Responders/evaluable	
	Sensitive relapse	Refractory disease
Topotecan	18% (30/168)	8% (6/75)
Irinotecan	28% (18/63)	3% (1/28)
Docetaxel	19% (9/47)	
Paclitaxel		29% (7/24)
Gemcitabine		14% (5/38)
Vinorelbine	17% (7/41)	0% (0/8)
Amrubicin	52% (23/44)	50% (8/16)

[a] Glisson BS. Semin Oncol 30: 72–78, 2003

The second line treatment of NSCLC and 1st line treatment in elderly patients are in categories for which single-agent chemotherapy should be the recommended option. It is necessary to test amrubicin for these categories. To date, amrubicin has been approved and licensed for 3-day administration, but a phase I clinical study of this administration method has only been conducted in previously untreated patients, and there is still a problem concerning whether the recommended dosage of 45 mg/m^2/day is tolerable in previously treated patients, especially in light of its strong myelotoxicity. On this point, Okamoto et al. recently conducted a phase I study of amrubicin in previously treated patients with lung cancer, and reported a recommended phase II dosage of amrubicin at 35 mg/m^2/day for three consecutive days every 3 weeks [20].

For ED-SCLC, based on the good results obtained from combination therapy with cisplatin, a randomized phase III study should be carried out involving a comparison with cisplatin–CPT-11 combination therapy. Other anticancer drugs that should be investigated for combination therapy include carboplatin, as well as the topoisomerase I inhibitors CPT-11 and topotecan, which have recently been playing major roles in the treatment of SCLC. Because no standard treatment has yet been established for SCLC that

recurs after the initial treatment, a possible target of amrubicin monotherapy is previously treated SCLC.

The clinical studies suggested above should be conducted for both NSCLC and SCLC; however, because amrubicin is strongly myelotoxic, special consideration should be taken if these drugs are used in combination. From this viewpoint, it is also important to examine the pharmacokinetic profile of amrubicin. There is only one report by Matsunaga et al. regarding the pharmacokinetics of amrubicin and its active metabolite amrubicinol in patients with lung cancer [21]. In this report, it was suggested that the area-under-the time curves of amrubicin and amrubicinol seemed to be associated with the hematologic toxicities, and interestingly interpatient variability in the enzymatic conversion of amrubicin to amrubicinol was small whereas a large interpatient variability in the clearance of amrubicin was observed [21].

Conclusion

Clinical studies of the novel anticancer agent amrubicin have only begun, and we as yet have little evidence to evaluate. However, there are high expectations for this agent in the trial to improve outcome for both NSCLC and SCLC patients. Many issues remain to be resolved, such as how to position this drug in the actual treatment of lung cancer. In order to resolve this and other issues in the future, many high-quality clinical studies are needed.

References

1. Yamaoka T, Hanada M, Ichii S et al (1998) Cytotoxicity of amrubicin, a novel 9-aminoanthracycline, and its metabolite amrubicinol on human tumor cells. Jpn J Cancer Res 89:1067–1073
2. Noguchi T, Ichii S, Yamaoka T et al (1998) In vivo efficacy and tumor-selective metabolism of amrubicin to its active metabolite. Jpn J Cancer Res 89:1055–1060
3. Suzuki T, Minamide S, Iwasaki T et al (1997) Cardiotoxicity of a new anthracycline derivative (SM5887) following intravenous administration to rabbits: comparative study with doxorubicin. Invest New Drugs 15:219–225
4. Morisada S, Yanagi Y, Noguchi T et al (1989) Antitumor activities of a novel 9-aminoanthracycline (SM5887) against mouse experimental tumors and human tumor xenografts. Jpn J Cancer Res 80:69–76
5. Noguchi T, Ichii S, Morisada S et al (1999) Evaluation of amrubicin with a 5 day administration schedule in a mouse model. Gan To Kagaku Ryoho 26:1305–1312
6. Hanada M, Mizuno S, Fukushima A et al (1998) A new antitumor agent amrubicin induces cell growth inhibition by stabilizing topoisomerase II-DNA complex. Jpn J Cancer Res 89:1229–1238
7. Inoue K, Ogawa M, Horikoshi N et al (1988) Phase I study of SM-5887, a new anthracycline derivative. Gan To Kagaku Ryoho 15:1771–1776
8. Inoue K, Matsumura A, Horikoshi N et al (1992) Phase I and pharmacokinetic study of SM-5887 by 5-day schedule. Gan To Kagaku Ryoho 19:477–482
9. Feld R, Wierzbicki R, Walde PLD et al (1992) Phase I–II study of high-dose epirubicin in advanced non-small-cell lung cancer. J Clin Oncol 10:297–303
10. Sugiura T, Ariyoshi Y, Negoro S et al (2005) Phase I/II study of amrubicin, a novel 9-aminoanthracycline, in patients with advanced non-small-cell lung cancer. Invest New Drugs 23:331–337
11. Sawa T, Yana T, Takada M et al (2006) Multicenter phase II study of amrubicin, 9-amino-anthracycline, in patients with advanced non-small-cell lung cancer (Study 1): West Japan Thoracic Oncology Group (WJTOG) trial. Invest New Drugs 24(2):151–158
12. Yana T, Negoro S, Takada M et al (2006) Phase II study of amrubicin in previously untreated patients with extensive-disease small cell lung cancer: West Japan Thoracic Oncology Group (WJTOG) study. Invest New Drugs 25:253–258
13. Ohe Y, Negoro S, Matsui K et al (2005) Phase I–II study of amrubicin and cisplatin in previously untreated patients with extensive-stage small-cell lung cancer. Ann Oncol 16:430–436
14. Noda K, Nishiwaki Y, Kawahara M et al (2005) Irinotecan plus cisplatin compared with etoposide plus cisplatin for extensive small-cell lung cancer. N Engl J Med 346:85–91
15. Onoda S, Masuda N, Seto T et al (2006) Phase II trial of amrubicin for treatment of refractory or relapsed small-cell lung cancer: Thoracic Oncology Research Group Study 0301. J Clin Oncol 24(34):5448–5453
16. Glisson BS (2003) Recurrent small cell lung cancer: update. Semin Oncol 30(1):72–78
17. von Pawel J, Schiller JH, Shepherd FA et al (1999) Topotecan versus cyclophosphamide, doxorubicin, and vincristine for the treatment of recurrent small-cell lung cancer. J Clin Oncol 17 (2):658–667
18. Holmes FA, Madden T, Newman RA et al (1996) Sequence-dependent alteration of doxorubicin pharmacokinetics by paclitaxel in a phase I study of paclitaxel and doxorubicin in patients with metastatic breast cancer. J Clin Oncol 14:2713–2721
19. Yanaihara T, Yokoba M, Masuda N et al (2007) Phase I and pharmacologic study of irinotecan and amrubicin in advanced non-small cell lung cancer. Cancer Chemother Pharmacol 59(4):419–427
20. Okamoto I, Hamada A, Matsunaga Y et al (2005) Phase I and pharmacokinetic study of amrubicin, a synthetic 9-aminoanthracycline, in patients with refractory or relapsed lung cancer. Cancer Chemother Pharmacol 19:1–7, July
21. Matsunaga Y, Hamada A, Okamoto I et al (2006) Pharmacokinetics of amrubicin and its active metabolite amrubicinol in lung cancer patients. Ther Drug Monit 28(1):76–82

Oncogene (2007) 26, 4025–4031

www.nature.com/onc

SHORT COMMUNICATION

CLCP1 interacts with semaphorin 4B and regulates motility of lung cancer cells

H Nagai[1,2,3], N Sugito[2], H Matsubara[1,3], Y Tatematsu[2], T Hida[4], Y Sekido[2], M Nagino[3], Y Nimura[3], T Takahashi[1,2] and H Osada[2]

[1]Division of Molecular Carcinogenesis, Center for Neurological Diseases and Cancer, Nagoya University Graduate School of Medicine, Nagoya, Japan; [2]Division of Molecular Oncology, Aichi Cancer Center Research Institute, Nagoya, Japan; [3]Division of Surgical Oncology, Department of Surgery, Nagoya University Graduate School of Medicine, Nagoya, Japan and [4]Department of Pulmonary Medicine, Aichi Cancer Center Hospital, Nagoya, Japan

We previously established a highly metastatic subline, LNM35, from the NCI-H460 lung cancer cell line, and demonstrated upregulation of a novel gene, *CLCP1* (CUB, LCCL-homology, coagulation factor V/VIII homology domains protein), in LNM35 and lung cancer specimens. In this study, we focused on the potential roles of that gene in cancer metastasis. First, we established stable LNM35 RNAi clones, in which *CLCP1* expression was suppressed by RNAi, and found that their motility was significantly reduced, although growth rates were not changed. Next, *in vitro* selection of a phage display library demonstrated that a phage clone displaying a peptide similar to a sequence within the Sema domain of semaphorin 4B (SEMA4B) interacted with LNM35. Immunoprecipitation experiments confirmed interaction of CLCP1 with SEMA4B, regulation of CLCP1 protein by ubiquitination and proteasome degradation enhanced in the presence of SEMA4B. These results are the first to indicate that CLCP1 plays a role in cell motility, whereas they also showed that at least one of its ligands is SEMA4B and that their interaction mediates proteasome degradation by CLCP1. Although the physiological role of the interaction between CLCP1 and SEMA4B remains to be investigated, this novel gene may become a target of therapy to inhibit metastasis of lung cancers.
Oncogene (2007) **26**, 4025–4031; doi:10.1038/sj.onc.1210183; published online 8 January 2007

Keywords: CLCP1; SEMA4B; lung cancer

Lung cancer is the leading cause of cancer-related death in developed countries. Despite a considerable body of knowledge regarding the molecular mechanisms of development and progression of lung cancer, most patients eventually die because of widespread metastases. Thus, it is considered important to identify the molecules that play crucial roles in cell motility/invasion and metastasis in order to significantly reduce mortality rates. For this purpose, we established a highly metastatic subline, LNM35, from the NCI-H460 human lung cancer cell line (Kozaki *et al.*, 2000), which showed upregulation of various proinflammatory cytokines and angiogenic chemotactic chemokines in comparison to a representative low metastatic clone of the parental line (Kozaki *et al.*, 2001). Based on this profiling analysis, we also identified and characterized a novel gene, *CLCP1* (CUB, LCCL-homology, coagulation factor V/VIII homology domains protein), also termed endothelial and smooth muscle cell-derived neuropilin-like molecule (*ESDN*)/discoidin, CUB and LCCL domain containing 2 (*DCBLD2*) (Kobuke *et al.*, 2001), that demonstrated upregulated expression in LNM35 as well as in a significant fraction of lung cancers, especially lymph node metastases (Koshikawa *et al.*, 2002). The *CLCP1* gene encodes a 775-amino-acid protein with structural similarities to neuropilins, cell surface receptors for vascular endothelial growth factor $(VEGF)_{165}$ and semaphorins (Koshikawa *et al.*, 2002), which were originally identified as neural axon repulsion signaling molecules active in axon guidance. Some class III semaphorins function as tumor suppressors, whereas one class IV member may promote tumor progression through induction of angiogenesis (Kruger *et al.*, 2005). In the present study, we explored the functions of CLCP1 in tumor progression and metastasis, and found that knock down reduces tumor cell motility. Using the phage peptide library, we also obtained evidence that at least one ligand of CLCP1, Sema domain of the human semaphorin 4B (SEMA4B), is a class IV semaphorin that may be also involved in the regulation of cell motility through its induction of CLCP1 degradation.

Observation of a high expression of *CLCP1* in lung cancer specimens prompted us to examine its functional contribution to the high metastatic properties of LNM35 cells. We generated several small interfering RNA (siRNA) constructs expressing short hairpin RNAs targeting CLCP1, and found two siRNA sites (siCLCP1–2 and siCLCP1–3) that were able to effectively knock down CLCP1 expression in 293T cells co-transfected with a CLCP1 expression vector and an

Correspondence: Dr H Osada, Division of Molecular Oncology, Aichi Cancer Center Research Institute, 1-1 Kanokoden, Chikusa-ku, Nagoya 464-8681, Japan.
E-mail: hosada@aichi-cc.jp
Received 5 June 2006; revised 30 October 2006; accepted 2 November 2006; published online 8 January 2007

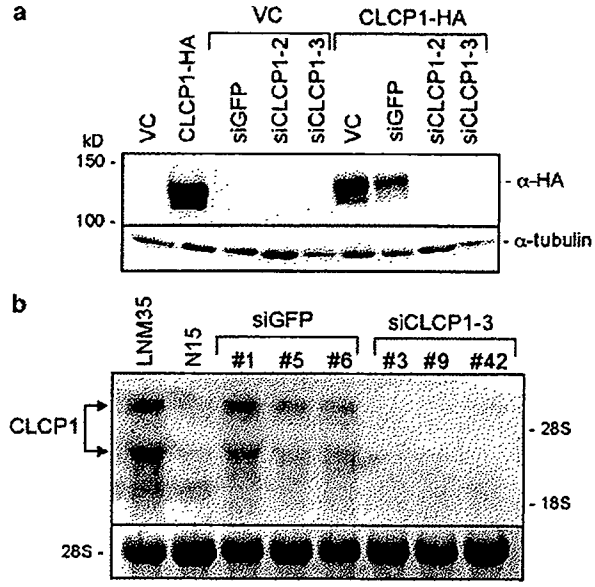

Figure 1 CLCP1 expression and establishment of LNM35-RNAi clones. (a) Immunoblotting of CLCP1-RNAi transfectants. RNAi plasmid vectors were constructed by insertion of the H1 promoter 5′ upstream of the CMV promoter driving a neomycin-resistant gene (pH1-RNA neomycin). CLCP1-RNAi sites were designed at 1196–1214 nt and 1935–1953 nt of *CLCP1* ORFs for siCLCP1–2 and siCLCP1–3, respectively. A blast homology search did not indicate any strong homology for these RNAi sites. 293T cells were transfected with each RNAi-vector along with the HA-tagged CLCP1 expression vector (Koshikawa *et al*., 2002). A control RNAi construct for the GFP gene, siGFP, was also used. Note the significant reduction of expression of CLCP1 protein observed with siCLCP1–2 and siCLCP1–3. (b) Northern blotting of stable LNM35-RNAi clones. LNM35 was transfected with siCLCP1–3 RNAi constructs and selected with neomycin (1 mg/ml) for 2 weeks. The expression of endogenous *CLCP1* transcripts was almost undetectable in the LNM35 siCLCP1–3 clones (nos. 3, 9 and 42), whereas the high level of expression of *CLCP1* was not affected in control clones that received the siGFP construct. Note the significant difference in *CLCP1* expression level between LNM35 and the parental line N15.

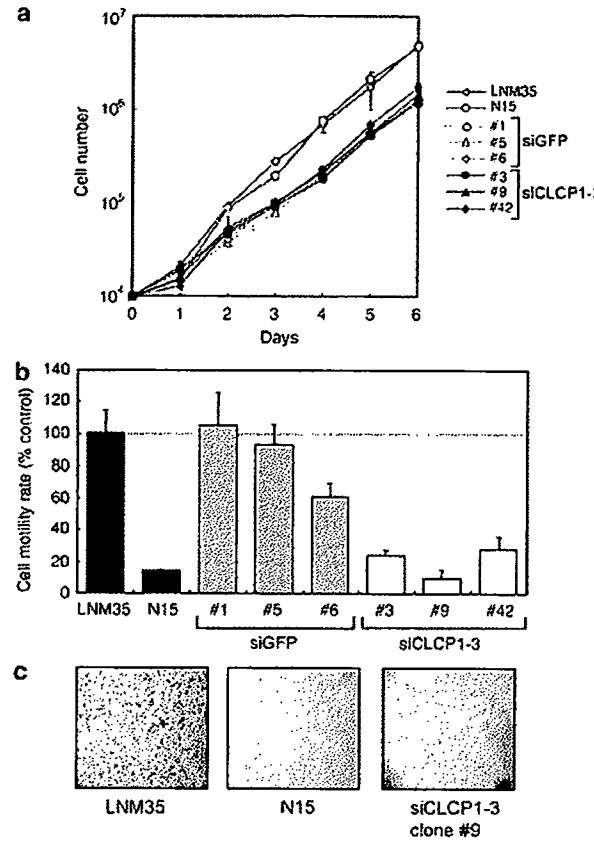

Figure 2 Cell proliferation and motility of LNM35 RNAi clones. (a) Cell proliferation assay. Stable clones were plated at 1×10^4 per dish in RPMI1640 medium with 5% fetal bovine serum and neomycin, then cell numbers were counted each day with a Z1 Coulter Counter (Beckman Coulter, Fullerton, CA, USA). The growth rates of the siCLCP1–3 clones were quite similar to those of the control siGFP clones, (b, c) *in vitro* motility assay. Motility of the RNAi clones was studied using transwell chambers, as described previously (Kozaki *et al*., 2001) and found to be significantly decreased in all three siCLCP1–3 clones (white bars), whereas the siGFP clones (hatched bars) retained their high levels of motility. (c) A number of migrated cells were observed among the LNM35 cells by Giemsa staining, whereas there were very few N15 or siCLCP1 cells ($\times 40$ magnification). The small dots represent 8 μm-sized transwell chamber pores.

siRNA vector (Figure 1a). To determine whether these findings were associated with decreased cell growth and/or motility of LNM35, we established stable LNM35 transfectant clones. Northern blotting (Figure 1b) revealed that the expression level of *CLCP1* in siCLCP1–3 clones nos. 3, 9 and 42 was significantly reduced to the level of the parental subclone of NCI-H460, N15, whereas *CLCP1* expression was not affected in control siGreen fluorescent protein (siGFP) clones (Supplementary Figure 3). Thereafter, these three siCLCP1–3 clones were employed for further biological analyses.

Cell growth rate was studied and the growth rates of the siCLCP1–3 clones were quite similar to those of siGFP clones (Figure 2a), suggesting that CLCP1 expression is not involved in the regulation of cell growth in LNM35 cells. However, motility was significantly decreased in the siCLCP1–3 clones, whereas the siGFP clones retained high motility (Figure 2b and c), implying that CLCP1 has an effect to enhance cell migration.

Concurrently with the above analyses, we searched for cell surface molecules specific to LNM35 using a phage display method in order to identify the molecular mechanisms of the high motility/invasion ability of LNM35. One of the peptides enriched with this method was SAYIPDS, whose sequence was nearly identical to that of SAYIPES within the SEMA4B gene (Figure 3a). This domain is known to be crucial for interactions with other proteins. CLCP1 has structural similarities to neuropilins, which function as cell surface receptors for semaphorins, therefore, we speculated that the selected peptide and SEMA4B might interact with CLCP1. We compared the interactions of the phage with LNM35 (high CLCP1 expression) and N15 (low CLCP1 expression). When cells were incubated with the phage displaying the

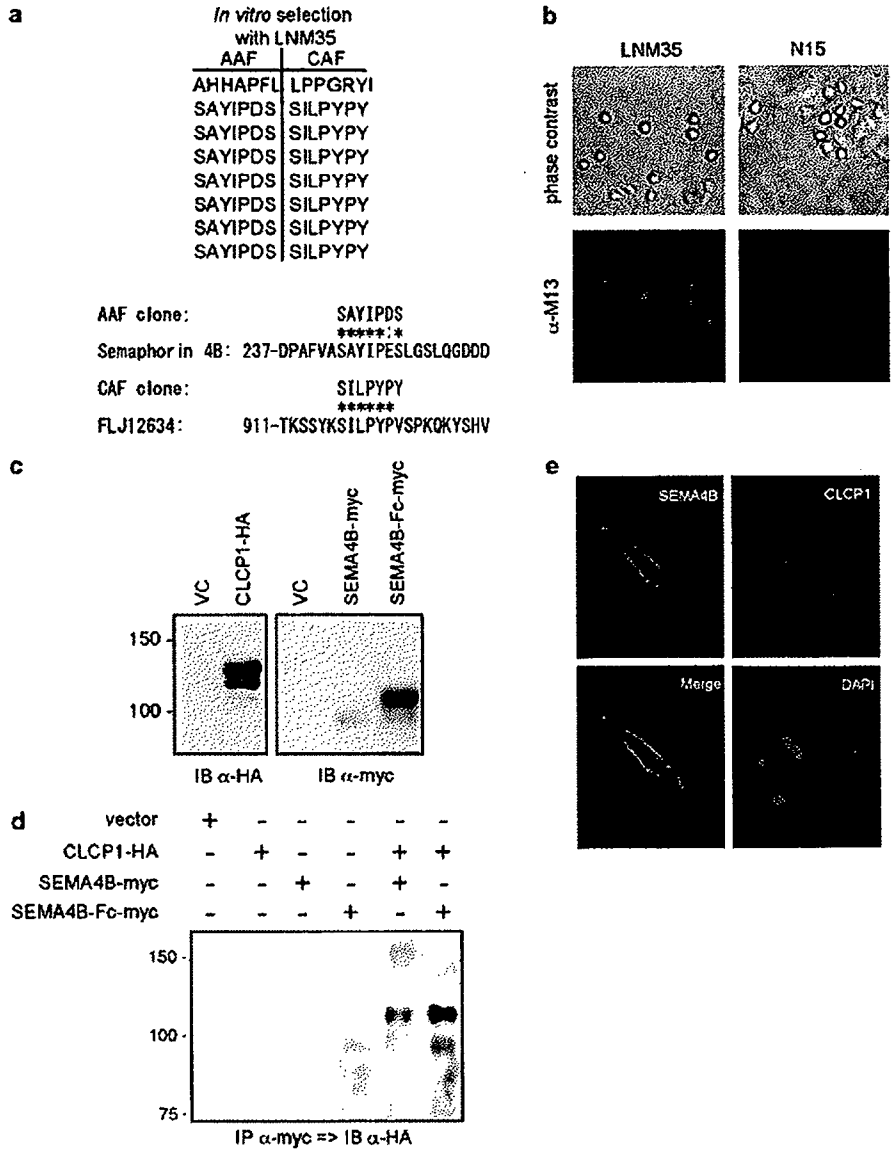

Figure 3 CLCP1 interacts with SEMA4B. (a) *In vitro* selection of LNM35 cells using a phage display library (PhD-7 Phage Display Peptide Library, New England Biolabs, Ipswich, MA, USA). For each selection, $1–2 \times 10^{11}$ PFU of phage particles were overlaid on LNM35 cells. After incubation and washing, attached phages were eluted with acid elution buffer (acid-associated fraction (AAF)). Tightly associated phages were also recovered after cell lysis (cell-associated fraction (CAF)). The phages were amplified following infection with bacteria and rounds of incubation-elution-amplification were repeated. Seven of the eight AAF phage clones sequenced after four rounds of selection contained the SAYIPDS peptide, which was nearly identical to the sequence SAYIPES within the SEMA4B gene. CAF phage results indicated the sequence of a hypothetical protein FLJ12634. (b) Immunofluorescence of phages attached to LNM35. Both LNM35 (with high CLCP1 expression) and N15 (with low CLCP1 expression) cells were incubated with phages displaying the SAYIPDS peptide. After washing and fixation, cell-attached phages were immuno-stained with the monoclonal antibody against M13 procoat protein (GE Healthcare Bio-Science, Piscataway, NJ, USA) and Alexa488-conjugated anti-mouse IgG (Invitrogen, Carlsbad, CA, USA). Note the stronger binding of the SAYIPDS phage with LNM35 as compared to that with N15. (**c**, **d**) Co-immunoprecipitation of CLCP1 with SEMA4B. The SEMA4B cDNA clone, KIAA1745, was kindly provided by Kazusa DNA Research Institute. For the SEMA4B-myc expression construct, the SEMA4B ORF was introduced into pcDNA3 (Invitrogen) together with myc-tag at its C-terminus. For the SEMA4B-Fc-myc construct, a 1720-bp *Sac*II-*Bam*HI fragment of KIAA1745 containing only the Sema domain was fused to the cDNA of the human IgG1 Fc portion in the pcDNA vector with an myc-tag at the C-terminus of the Fc portion. SEMA4B-myc or SEMA4B-Fc-myc was co-transfected with CLCP1-HA into 293T cells, and the generated proteins were immunoprecipitated with mouse monoclonal anti-myc-tag antibody 9E10. Immunoblots of these precipitates with rabbit anti-HA antibodies clearly demonstrated co-immunoprecipitation of CLCP1 with SEMA4B proteins. (e) Immunofluorescence of SEMA4B and CLCP1. The A549 lung cancer cell line was transfected with SEMA4B-myc and CLCP1-HA expression vectors, then stained with Alexa Fluor dye-labeled secondary antibodies (Invitrogen) after MG-132 treatment, as performed in Figure 4b and c. Observation with a confocal microscope (Olympus, Tokyo, Japan) showed both CLCP1 and SEMA4B to be mainly localized on the cell surface membrane, with colocalization clearly observed in merged images.

SAYIPDS peptide and then immuno-stained with the anti-M13 antibody against the phage particle, LNM35 staining was more intense than that of N15 (Figure 3b). Next, the indicated interaction between CLCP1 and SEMA4B was studied using an myc-tagged full-length SEMA4B construct, as well as an myc-tagged SEMA4B-Fc fusion construct consisting of the SEMA4B Sema domain and immunoglobulin (Ig)G Fc portion. After co-transfection with hemagglutinin (HA)-CLCP1 into 293T cells, anti-HA immunoblotting of anti-myc immunoprecipitates clearly demonstrated co-precipitation of CLCP1 with SEMA4B or SEMA4B-Fc (Figure 3d). Further, colocalization of CLCP1 and SEMA4B proteins on cell surface membranes was demonstrated by immunofluorescence analysis (Figure 3e).

HA-tagged CLCP1 demonstrated two sizes, 130 and 110 kDa, which were both larger than the predicted molecular mass of 80 kDa. We previously speculated that post-translational modifications such as glycosylation might account for this discrepancy (Koshikawa *et al.*, 2002), as is the case with most transmembrane proteins. To confirm this, 293T cells were transfected with HA-CLCP1 and then treated with tunicamycin, which blocks the first step in the biosynthesis of N-linked oligosaccharides. Tunicamycin treatment reduced the amounts of both the 130- and 110-kDa bands in a dose-dependent manner. Simultaneously, a novel 80-kDa band appeared (Figure 4a), indicating that CLCP1 protein is indeed post-translationally modified by glycosylation, resulting in 130- and 110-kDa-sized proteins, which might be properly processed into transmembrane proteins.

We found that the intensity of the CLCP1 protein band was significantly weaker after CLCP1-SEMA4B co-transfection as compared to with CLCP1 transfection alone (Figure 4b), and subsequently attempted to determine whether SEMA4B caused degradation of CLCP1 protein in a proteasome-dependent manner. When 293T cells were transfected with CLCP1 and/or SEMA4B, and then treated with MG-132, a specific inhibitor of proteasomes, anti-HA immunoblots indicated an increased intensity of both the 130- and 110-kDa bands in the CLCP1 transfectants (Figure 4b, lanes 3 and 4), suggesting that CLCP1 alone was originally regulated by proteasome degradation. However, CLCP1–SEMA4B and CLCP1–SEMA4B-Fc co-transfection were both associated with a significantly reduced intensity of the largest band (130 kDa) (Figure 4b, lanes 5 and 7). Similarly, MG-132 treatment enhanced the intensity of the 110-kDa band (Figure 4b, lanes 4, 6 and 8). However, the 130-kDa band was only moderately restored with CLCP1–SEMA4B co-transfection (Figure 4b, lane 6) and not recovered at all with CLCP1–SEMA4B-Fc co-transfection (Figure 4b, lane 8). In Figure 4c, the size of the co-immunoprecipitated CLCP1 isoform was compared with that of CLCP1 proteins in cell lysates derived from transfectants treated with or without MG-132 or another proteasome inhibitor, lactacystin, which was effective for a Smad4 mutant (Yanagisawa *et al.*, 2000) (Supplementary Figures 1 and 2). The main co-precipitated CLCP1 isoform appeared to be a 110-kDa isoform, even in samples treated with proteasome inhibitors. These findings suggest that the degradation of the 130-kDa band induced by SEMA4B proteins may be too severe to be inhibited by the applied concentration of MG-132. Nevertheless, even with higher concentrations of proteasome inhibitors, full restoration of the 130-kDa band was not obtained (Supplementary Figure 2), suggesting that the interactions with SEMA4B proteins, especially SEMA4B-Fc, may not only induce degradation, but also affect full glycosylation of CLCP1. We also examined the ubiquitination status of CLCP1 using P4D1 monoclonal antibodies that recognize both monoUb and polyUb (Figure 4d). Although ubiquitinated CLCP1 was readily detected in cells co-transfected with the empty vector (Figure 4d, lane 4), the ubiquitination of CLCP1 was significantly increased following co-transfection with SEMA4B (Figure 4d, lane 6). These results suggest that CLCP1–SEMA4B interactions induce significant degradation of CLCP1 proteins, especially 130-kDa fully-glycosylated CLCP1.

This present results indicated that the neuropilin-like protein CLCP1 is upregulated in highly metastatic lung cancer cells and may promote cell motility, possibly resulting in promotion of metastasis. We also found that SEMA4B is a possible ligand of CLCP1, as CLCP1–SEMA4B interaction caused CLCP1 degradation. CLCP1/ESDN was also reported to be expressed by vascular smooth muscle cells, as well as upregulated by platelet-derived growth factor-BB stimulation and vascular injury, suggesting that it modulates growth-promoting signals (Kobuke *et al.*, 2001). Class III semaphorins interact with neuropilins through binding of their Sema and CUB or FV/VIII domains, respectively. Although the interaction domains of CLCP1 and SEMA4B have yet to be determined, it is conceivable that the Sema domain of SEMA4B interacts with CUB and FV/VIII domains of CLCP1. The fact that the sequence within the Sema domain was enriched with the phage display selection in LNM35 expressing CLCP1 provides support for this speculation.

Cell migration is a multistep process that includes leading edge protrusion, focal contact formation and actomyosin-dependent cell contraction, and also involves small guanosine triphosphatase (GTPase) and integrins. Small GTPases, including Rho, Rac and Cdc42, control cell motility by regulating actin and microtubule dynamics (Friedl and Wolf, 2003). Semaphorins and neuropilins make protein complexes with plexins, which regulate the activities of small GTPases through interactions with these small GTPases and Rho-guanine nucleotide exchange factor (Kruger *et al.*, 2005). In addition, a recent report showed that Sema4D-plexin-B1 interaction downregulates R-Ras activity through the endogenous GTPase-activating protein activity of plexin-B1, resulting in inhibition of focal contact mediated by integrins (Oinuma *et al.*, 2004). Therefore, to understand the molecular mechanisms underlying the regulation of cell motility by CLCP1, it is important to clarify whether CLCP1 signaling has any effects on the activities of these small GTPases and integrins.

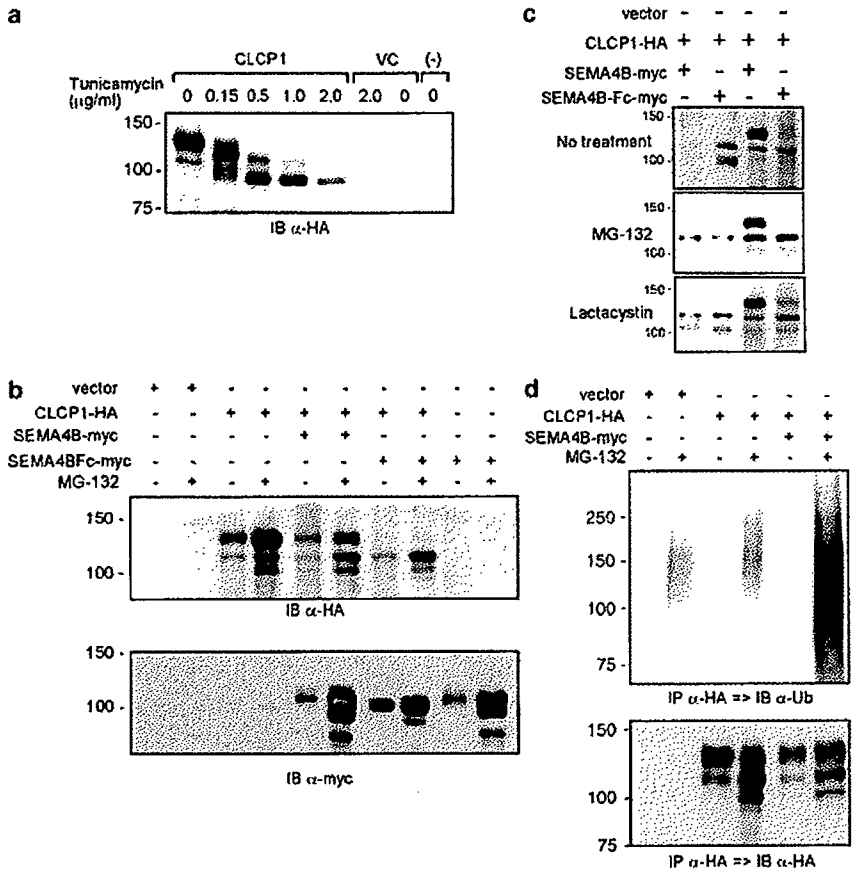

Figure 4 Post-translational modification of CLCP1 protein. (a) *N*-glycosylation of CLCP1. 293T cells were transfected with the CLCP1-HA vector and then treated with an *N*-linked glycosylation inhibitor, tunicamycin (Wako Pure Chemical Industries Ltd., Osaka, Japan), for 24 h at the indicated concentrations. Reductions in the amounts of both the 130- and 110-kDa bands resulted, with simultaneous appearance of a novel 90-kDa band similar to the predicted size in a dose-dependent manner. (b) Degradation of CLCP1 protein. 293T cells were transfected with CLCP1-HA, SEMA4B-myc and/or SEMA4B-Fc-myc, then treated with a proteasome inhibitor, MG-132 (SIGMA-ALDRICH, St Louis, MO, USA), at 10 μM for 24 h. The expression levels of CLCP1 and SEMA4B proteins were then investigated using anti-HA and anti-myc antibodies. Without MG-132 treatment, the CLCP1 protein band was significantly weaker after CLCP1/SEMA4B or CLCP1/SEMA4B-Fc co-transfection (lanes 5, 7) than with CLCP1 transfection alone (lane 3). MG-132 treatment enhanced the intensity of the CLCP1 protein band in co-transfections (lanes 6, 8) and also with CLCP1 transfection alone (lane 4). Proteasome-dependent degradations of SEMA4B proteins were also observed. (c) Analysis of the co-immunoprecipitated isoform of CLCP1. Immunoprecipitation and immunoblotting of CLCP1/SEMA4B and CLCP1/SEMA4B-Fc co-transfected cells were conducted, the same as in Figure 3d. Transfected cells were treated with MG-132 (10 μM) or another proteasome inhibitor, lactacystin (15 μM, Wako Pure Chemical Industries Ltd.). Immunoprecipitated proteins (lane 1, 2) were run with cell lysates before immunoprecipitation (lane 3, 4). The main immunoprecipitated CLCP1 isoform appeared to be the same 110-kDa isoform noted in (a). (d) Ubiquitination of CLCP1. As in (b), 293T cells were transfected and treated with MG-132. Then, CLCP1 protein was immunoprecipitated with the anti-HA antibody and analysed with the anti-ubiquitin antibody, P4D1 (Santa Cruz Biotechnology, Inc., Santa Cruz, CA, USA). Ubiquitination of CLCP1 was readily detected following transfection of CLCP1 alone (lane 4) and significantly increased by co-transfection with SEMA4B (lane 6).

In a previous study, SEMA3A inhibited the migration and spread of a breast cancer cell line, MDA-MB-231, which expresses neuropilin-1 and plexin-A1, whereas another ligand of neuropilin-1, $VEGF_{165}$, was shown to compete with SEMA3A and abrogate its inhibitory effect (Bachelder *et al*., 2003). CLCP1 may also interact with other ligand molecules, which might regulate cell motility in competition with SEMA4B. In the present study, we also examined the involvement of cyclooxygenase 2 (COX-2) in *CLCP1* expression (Supplementary Figure 4), because a previous study showed that COX-2 was upregulated in LNM35 cells and contributed to their highly metastatic characteristics (Kozaki *et al*., 2000). We found that nimesulide, a COX-2 inhibitor, repressed *CLCP1* mRNA levels, suggesting a functional association between COX-2 activation and *CLCP1* overexpression in LNM35 cells.

SEMA3B and *SEMA3F*, which are localized at the 3p21.3 locus, are frequently deleted in lung cancers and have been found to suppress tumor cell proliferation (Tse *et al*., 2002; Xiang *et al*., 2002; Castro-Rivera *et al*., 2004). In contrast, class IV semaphorins do not show

such a tumor suppressor function, whereas Sema4D was originally reported to promote B-cell survival and T-cell activation. Another study showed that Sema4D induces angiogenesis, which was mediated by the coupling of its high-affinity receptor plexin-B1 with the Met tyrosine kinase (Conrotto *et al.*, 2005). In addition, class IV semaphorins frequently have PDZ {PSD (postsynaptic density protein) 95, DlgA (Discs large A), and ZO (zonula occludens) 1)} domain-binding motifs at their C-termini, through which they may function as receptors by mediating signal transfers through their intracellular domains. SEMA4B, 4C and 4F have been shown to interact with the PDZ domains of PSD-95 (Inagaki *et al.*, 2001; Burkhardt *et al.*, 2005), whereas SEMA4D was found to associate with CD45 protein tyrosine phosphatase (Herold *et al.*, 1996). Therefore, SEMA4B might function as a CLCP1 receptor. Sema3A–neuropilin interactions induce neuropilin-1 endocytosis, which is mediated by L1-CAM (Fournier *et al.*, 2000; Castellani *et al.*, 2004), which in turn modulates growth cone sensitivity to semaphorin repulsion signals. CLCP1 degradation after CLCP1–SEMA4B interaction may indicate an induction of CLCP1 endocytosis by SEMA4B.

In conclusion, the present results indicate that CLCP1 and its interactions with ligands including SEMA4B may become molecular targets for therapeutic inhibition of metastasis. In addition to CLCP1-siRNA, the suppression of CLCP1 functions with dominant-negative CLCP1 or negatively regulating ligands might inhibit *in vitro* motility and, consequently, *in vivo* metastasis of cancer cells. Fine mapping of the interacting regions between CLCP1 and SEMA4B may indicate concrete molecular targets. Although a full understanding of the biological roles of CLCP1 and SEMA4B remains to be achieved, further investigations of CLCP1 functions should provide novel and useful strategies to improve the clinical prognosis of lung cancer patients by facilitating the suppression of metastasis.

Acknowledgements

This work was supported in part by a Grant-in-Aid for Scientific Research on Priority Areas from the Ministry of Education, Culture, Sports, Science and Technology of Japan, a Grant-in-Aid for Scientific Research (B) and (C) from the Japan Society for the Promotion of Science, and a Grant-in-Aid for the Second Term Comprehensive Ten-Year Strategy for Cancer Control from the Ministry of Health and Welfare, Japan. We thank Kazusa DNA Research Institute for the SEMA4B cDNA clone, KIAA1745.

References

Bachelder RE, Lipscomb EA, Lin X, Wendt MA, Chadborn NH, Eickholt BJ *et al.* (2003). Competing autocrine pathways involving alternative neuropilin-1 ligands regulate chemotaxis of carcinoma cells. *Cancer Res* **63**: 5230–5233.

Burkhardt C, Muller M, Badde A, Garner CC, Gundelfinger ED, Puschel AW. (2005). Semaphorin 4B interacts with the post-synaptic density protein PSD-95/SAP90 and is recruited to synapses through a C-terminal PDZ-binding motif. *FEBS Lett* **579**: 3821–3828.

Castellani V, Falk J, Rougon G. (2004). Semaphorin3A-induced receptor endocytosis during axon guidance responses is mediated by L1 CAM. *Mol Cell Neurosci* **26**: 89–100.

Castro-Rivera E, Ran S, Thorpe P, Minna JD. (2004). Semaphorin 3B (SEMA3B) induces apoptosis in lung and breast cancer, whereas VEGF165 antagonizes this effect. *Proc Natl Acad Sci USA* **101**: 11432–11437.

Conrotto P, Valdembri D, Corso S, Serini G, Tamagnone L, Comoglio PM *et al.* (2005). Sema4D induces angiogenesis through Met recruitment by Plexin B1. *Blood* **105**: 4321–4329.

Fournier AE, Nakamura F, Kawamoto S, Goshima Y, Kalb RG, Strittmatter SM. (2000). Semaphorin3A enhances endocytosis at sites of receptor-F-actin colocalization during growth cone collapse. *J Cell Biol* **149**: 411–422.

Friedl P, Wolf K. (2003). Tumour-cell invasion and migration: diversity and escape mechanisms. *Nat Rev Cancer* **3**: 362–374.

Herold C, Elhabazi A, Bismuth G, Bensussan A, Boumsell L. (1996). CD100 is associated with CD45 at the surface of human T lymphocytes. Role in T cell homotypic adhesion. *J Immunol* **157**: 5262–5268.

Inagaki S, Ohoka Y, Sugimoto H, Fujioka S, Amazaki M, Kurinami H *et al.* (2001). Sema4c, a transmembrane semaphorin, interacts with a post-synaptic density protein, PSD-95. *J Biol Chem* **276**: 9174–9181.

Kobuke K, Furukawa Y, Sugai M, Tanigaki K, Ohashi N, Matsumori A *et al.* (2001). ESDN, a novel neuropilin-like membrane protein cloned from vascular cells with the longest secretory signal sequence among eukaryotes, is up-regulated after vascular injury. *J Biol Chem* **276**: 34105–34114.

Koshikawa K, Osada H, Kozaki K, Konishi H, Masuda A, Tatematsu Y *et al.* (2002). Significant up-regulation of a novel gene, CLCP1, in a highly metastatic lung cancer subline as well as in lung cancers *in vivo*. *Oncogene* **21**: 2822–2828.

Kozaki K, Koshikawa K, Tatematsu Y, Miyaishi O, Saito H, Hida T *et al.* (2001). Multi-faceted analyses of a highly metastatic human lung cancer cell line NCI-H460-LNM35 suggest mimicry of inflammatory cells in metastasis. *Oncogene* **20**: 4228–4234.

Kozaki K, Miyaishi O, Tsukamoto T, Tatematsu Y, Hida T, Takahashi T *et al.* (2000). Establishment and characterization of a human lung cancer cell line NCI-H460-LNM35 with consistent lymphogenous metastasis via both subcutaneous and orthotopic propagation. *Cancer Res* **60**: 2535–2540.

Kruger RP, Aurandt J, Guan KL. (2005). Semaphorins command cells to move. *Nat Rev Mol Cell Biol* **6**: 789–800.

Oinuma I, Ishikawa Y, Katoh H, Negishi M. (2004). The Semaphorin 4D receptor Plexin-B1 is a GTPase activating protein for R-Ras. *Science* **305**: 862–865.

Osada H, Tatematsu Y, Saito H, Yatabe Y, Mitsudomi T, Takahashi T. (2004). Reduced expression of class II histone deacetylase genes is associated with poor prognosis in lung cancer patients. *Int J Cancer* **112**: 26–32.

Tse C, Xiang RH, Bracht T, Naylor SL. (2002). Human Semaphorin 3B (SEMA3B) located at chromosome 3p21.3 suppresses tumor formation in an adenocarcinoma cell line. *Cancer Res* **62**: 542–546.

Xiang R, Davalos AR, Hensel CH, Zhou XJ, Tse C, Naylor SL. (2002). Semaphorin 3F gene from human 3p21.3 suppresses tumor formation in nude mice. *Cancer Res* **62**: 2637–2643.

Yanagisawa K, Uchida K, Nagatake M, Masuda A, Sugiyama M, Saito T *et al.* (2000). Heterogeneities in the biological and biochemical functions of Smad2 and Smad4 mutants naturally occurring in human lung cancers. *Oncogene* **19**: 2305–2311.

Supplementary Information accompanies the paper on the Oncogene website (http://www.nature.com/onc).

Clinical Trials Across Continents: Drug Development Challenges Regarding International Collaborations

By Nagahiro Saijo, MD, PhD

Overview: **A key consideration for global drug development and registration involves the acceptability of foreign clinical data in the different regions. Transcontinental trials could be possible if the clinical trials were done based on the same regulational standard against populations with acceptable ethnic differences. The problems of global drug development are discussed with special stress on pharmacodynamic and pharmacogenomic differences between white and Asian populations.**

THE CANCER burden in developed countries and resource-poor countries is sure to grow for three reasons. First, populations are rapidly increasing worldwide, especially in the majority of poor countries. Second, the elderly proportion is growing in most countries, and third, the incidence and mortality of cancers associated with smoking, diet, and obesity, have been increasing. Despite efforts at early detection and early surgery and radiotherapy, progress in the treatment of such cancers has been very slow, making the development of new anticancer drugs an extremely important and urgent issue to decrease cancer-related deaths worldwide. Resources are so limited that clinical trials need to be conducted as efficiently as possible, and one effort in that direction has been to conduct clinical trials on more than one continent to obtain adequate sample sizes in a short time. Anticancer drug development is a complex process that involves an interplay between industry, academia, government regulatory agencies, patient advocacy groups, and other stakeholders. The goal of anticancer drug development is to simultaneously launch new drugs on the market worldwide. Despite International Conference on Harmonisation (ICH) guideline G5 and the introduction of the bridging strategy, there are major gaps in the dates anticancer drugs become available on the market in different countries, and they do not seem to have dramatically improved.

PROBLEMS IN GLOBAL TRIALS OF ANTICANCER DRUGS

Factors in the complexity of global studies are differences between countries in medical practice, culture, ethnicity, and regulatory policies. The advantages of global development are shorter time for drug development; earlier introduction of new drugs and earlier availability to patients; cost reduction; and reduction in unnecessary exposure of patients to new drugs. The risks of global development are an increase in early-phase clinical trials of many compounds that may fail and may not proceed; low data quality; uncertainty of the acceptability of foreign data; and late-phase clinical trial failure because of unknown ethnic differences in response to the developing compounds.

Factors for success include strategies for global development and each country's development; global team behavior; cultural awareness and communications; and operational delivery. The leader of each global product team should be the worldwide product leader, and each country's leader should provide necessary strategic input into global teams.

The essential factors for team behaviors depend on trust, face-to-face contact, regular communications, open, honest discussion, and ability to challenge.

Factors for the success of global trials include coincidence of strategy for global and local development, the operating team, behaviors, cultural awareness and communications, and power for operational delivery. Ambiguous situations should be avoided by establishing formal rules and procedures. Operational delivery should be transparent, and mutual problems should be shared by global and local investigators. Regular contact by telephone is extremely important. A clear framework and decision making should be made for empowerment for delivery.

Although ICH good clinical practice (GCP) regulations have been distributed to major countries, there are still minor differences between ICH-GCP and local GCP. The requirements are different from local regulatory agencies on preclinical data before initiate clinical trials. Investigators' and patients' understanding of the importance of clinical trials differs by country. The infrastructure for clinical trials, such as the numbers of well-trained investigators and clinical research coordinators are sometimes inadequate, and sometimes there is poor information technology support and training in institutions. The process of applying for permission to conduct a clinical trial and institutional board review differ by institution and are sometimes complicated. English skills sometimes are very poor, and some investigators and institutions cannot accept English documents.

ETHNIC DIFFERENCES

It will be extremely difficult to conduct trials across continents if there are ethnic differences in pharmacokinetics, pharmacodynamics, pharmacogenetics, and pharmacogenomics. Ethnic differences have been clearly demonstrated in regard to only a few anticancer drugs, and progress in pharmacogenomic studies has led to the

From the National Cancer Center, Chiba-ken, Japan.
Author's disclosure of potential conflicts of interest is found at the end of this article.
Address reprint requests to Nagahiro Saijo, MD, PhD, National Cancer Center, Kashiwanoha 6-5-1, Kashiwa-shi, Chiba-ken, Japan; e-mail: nsaijo@east.ncc.go.jp.

1092-9118/07/177-179

identification of some of the mechanisms responsible for the ethnic differences.

EPIDERMAL GROWTH FACTOR RECEPTOR TYROSINE KINASE INHIBITOR

A phase I Japanese trial of gefitinib revealed five dramatic responders, and the response rate among the 36 patients accrued to the phase I trial was more than 25%. Subsequent global phase II trials, such as Iressa Dose Evaluation in Advanced Lung Cancer (IDEAL) I and IDEAL II, have yielded a higher response rate in a Japanese population (28%) than in a white population (10%).[1,2] In April 2004, extremely important data were reported suggesting that epidermal growth factor receptor (EGFR) mutations, especially deletion of exon 19 and the point mutation of exon 21, determine sensitivity to EGFR tyrosine kinase inhibitors (TKIs), such as gefitinib and erlotinib.[3,4] The frequency of EGFR mutations has been found to be significantly higher in Asian populations, including Japanese, than in whites (32% vs. 6%). This difference may explain the difference in response rate to EGFR TKIs. The frequency of EGFR mutations also correlated well with clinical factors, such as female sex, nonsmoker, and adenocarcinoma, which are closely related to the response to EGFR TKI.[5,6] The results of the global Iressa Survival Evaluation in Lung Cancer (ISEL) and National Cancer Institute of Canada Clinical Trials Group BR-21 studies also suggest ethnic differences in sensitivity to EGFR TKI.

The ISEL study is a large randomized controlled trial of gefitinib in patients at 210 centers across 28 countries, and the difference between survival time was not statistically significant difference (hazard ratio [HR] = 0.89; $p = 0.087$) between the gefitinib group and placebo group. However, there was a very clear difference in survival between two groups in the Asian population (HR = 0.66; $p = 0.012$), although it consisted of only 342 patients, whereas the survival curves of the gefitinib group and placebo group in the non-Asian population (HR = 0.99; $p = 0.364$) of 1,350 patients were superimposable. In the BR-21 study of erlotinib, the HR for overall survival in the Asian group (0.61) was significantly smaller than in the white group (0.79).[7] These results strongly suggest that EGFR TKIs are different drugs between Asian and whites indicating that different clinical trials of EGFR TKIs should be scheduled based on ethnic differences. Astra Zeneca has instituted the Iressa Pan Asian Study into Asian populations alone. Many global clinical trials have been initiated in Asian countries, including Japan, Korea, China, Taiwan, Singapore, and Thailand. The accrual spread is generally good. If the trials are limited to Asian countries, pharmacogenomic ethnic differences are thought to be small, if they exist at all.

COMMON ARM ANALYSIS

Two common analyses of paclitaxel/carboplatin therapy in advanced non-small cell lung cancer (NSCLC) were presented in American Society of Clinical Oncology Annual Meetings in 2004 and 2006.[8,9] The purpose of these analyses was to evaluate whether the results of cancer clinical trials conducted in Japan can be directly extrapolated to U.S. populations. Potential differences that may influence the results include trial design and conduct, study-specific criteria, patient demographics, and population-based pharmacogenomics. The purpose of common arm analysis is to demonstrate similarities and differences in patient characteristics and outcomes of the same treatment regimen in Japanese and United States trials in advanced-stage NSCLC, to provide a basis for standardization of study design/conduct, to facilitate interpretation of future trials, and to take the first step toward joint National Cancer Institute-sponsored studies in lung cancer between the two countries.

The trials chosen for this analysis were the Four-Arm Cooperative Study (FACS),[10] Japan Multicenter Trial Organization (JMTO), and Southwest Oncology Group (SWOG) lung programs.[11] The conditions for selection were separate phase III trials, but with an identical common treatment regimen in each, prospective design and conduct, common eligibility and staging, and common response and toxicity criteria. SWOG 0003 was a phase III trial of paclitaxel (225 mg/m^2) and carboplatin (area under the time-concentration curve [AUC] = 6) with or without tirapazamine in advanced NSCLC. The FACS trial compared four arms: irinotecan and cisplatin (reference regimen), paclitaxel (200 mg/m^2) and carboplatin (AUC = 6), gemcitabine and cisplatin, and vinorelbine and cisplatin. The JMTO trial was a phase III trial comparing paclitaxel (225 mg/m^2) and carboplatin (AUC = 6) with gemcitabine/vinorelbine followed by docetaxel. In each trial paclitaxel and carboplatin was administered every 3 weeks. Patients were evenly distributed between arms in regard to age, sex, stage, and histology.

Treatment delivery consisted of a median number of cycles of three, four, and four in the FACS trial, S0003 trial, and JMTO trial, respectively, and the percentage of patients who received more than three cycles was significantly lower in the FACS trial than in the S0003 trial. The JMTO LC00–03 trial whose frequency dose was reduced was significantly higher than in the S0003 trial, although the percentage of patients who received more than three cycles was the same. The frequencies of grade 4 neutropenia and febrile neutropenia in the toxicity analysis were significantly higher in the FACS trial and LC00–03 trial than in the S0003 trial, but grade 3 to 4 neuropathy was more frequent in the S0003 trial and LC00–03 trial than in the FACS trial. The response rates in the three trials ranged from 32% to 36% and were almost the same. Progression-free survival time, median survival time, and 1-year survival rates were significantly better in the Japanese trials than in the S0003 trial. This common arm analysis shows great similarities in patient characteristics in the FACS, LC00–03 trial, and S0003 trial. The differences in toxicities may be due to differences in cumulative paclitaxel dose (neuropathy) and/or population-based pharmacogenomics (increased neutropenia and febrile neutropenia in the FACS trial despite lower paclitaxel doses). Survival with paclitaxel/carboplatin was

significantly better in the Japanese trials, although the response rates were equivalent.

The findings discussed here suggest that possible pharmacogenomic differences in drug disposition should be carefully considered in clinical trials across continents.

Sample collection for a pharmacogenomic analysis of taxanes has been completed in Japan. Single nucleotide polymorphism data for key enzyme/protein in the metabolism of taxanes have been obtained, and pharmacokinetics and pharmacodynamics data have also been collected. Differential analysis of the pharmacogenomics of the response to taxanes in the United States and Japan may make it possible to solve the problems of pharmacogenomic differences in clinical trials across continents.

Author's Disclosures of Potential Conflicts of Interest

Author	Employment or Leadership Positions (Commercial Firms)	Consultant or Advisory Role	Stock Ownership	Honoraria	Research Funding	Expert Testimony	Other Remuneration
Nagahiro Saijo			Takeda	Janssen-Cilag; Chugai; Kirin; Takeda; Eisai, Inc; Lilly Oncology; Merck; AstraZeneca			

REFERENCES

1. Herbst RS, Maddox AM, Rothenberg ML, et al. Selective oral epidermal growth factor receptor tyrosine kinase inhibitor ZD1839 is generally well-tolerated and has activity in NSCLC and other solid tumors: Results of a phase I trial. *J Clin Oncol.* 2002;20:3815-3825.

2. Fukuoka M, Yano S, Giaccone G, et al. Multi-institutional randomized phase II trial of gefitinib for previously treated patients with advanced NSCLC (the IDEAL I trial). *J Clin Oncol.* 2003;21:2237-2246.

3. Lynch TJ, Bell DW, Sordella R, et al. Activating mutations in the epidermal growth factor receptor underlying responsiveness of non-small-cell lung cancer to gefitinib. *N Engl J Med.* 2004;350:2129-2139.

4. Paez JG, Janne PA, Lee JC, et al. EGFR mutations in lung cancer: Correlation with clinical response to gefitinib therapy. *Science.* 2004;304: 1497-1500.

5. Mitsudomi T, Kosaka T, Endoh H, et al. Mutations of the epidermal growth factor receptor gene predict prolonged survival after gefitinib treatment in patients with non-small-cell lung cancer with postoperative recurrence. *J Clin Oncol.* 2005;23:2513-2520.

6. Takano T, Ohe Y, Sakamoto H, et al. Epidermal growth factor receptor gene mutations and increased copy numbers predict gefitinib sensitivity in patients with recurrent non-small-cell lung cancer. *J Clin Oncol.* 2005;23:6829-6837.

7. Thatcher N, Chang A, Parikh P, et al. Gefitinib plus best supportive care in previously treated patients with refractory advanced non-small-cell lung cancer: Results from a randomized, placebo-controlled, multicentre study (Iressa Survival Evaluation in Lung Cancer). *Lancet.* 2005;336:1527-1537.

8. Gandara DR, Ohe Y, Kubota K, et al. Japan-SWOG common arm analysis of paclitaxel/carboplatin in advanced stage non-small cell lung cancer (NSCLC): A model for prospective comparison of co-operative group trial. *J Clin Oncol.* 2004;22:618a (abstr 7007).

9. Crawley JJ, Furuse K, Gandara DR, et al. Japan-SWOG common arm analysis of paclitaxel/carboplatin therapy in advanced stage NSCLC. *J Clin Oncol.* 2006;24: (abstr 7050).

10. Ohe Y, Ohashi Y, Kubota K, et al. Randomized phase III study of cisplatin plus irinotecan versus carboplatin plus paclitaxel, cisplatin plus gemcitabine, and cisplatin plus vinorelbine for advannced NSCLC four arm cooperative study in Japan. *Ann Oncol. (in press).*

11. Williamson SK, Crowley JJ, Lara PN, et al. Paclitaxel/carboplatin (PC) vs PC + tirapazamine in advanced NSCLC: A phase III SWOG trial S0003. *J Clin Oncol.* 2003;20:9097-9104.

CYP2C8 haplotype structures and their influence on pharmacokinetics of paclitaxel in a Japanese population

Yoshiro Saito[a], Noriko Katori[a], Akiko Soyama[a], Yukiko Nakajima[a], Takashi Yoshitani[a], Su-Ryang Kim[a], Hiromi Fukushima-Uesaka[a], Kouichi Kurose[a], Nahoko Kaniwa[a], Shogo Ozawa[a], Naoyuki Kamatani[b], Kazuo Komamura[g,h], Shiro Kamakura[h], Masafumi Kitakaze[h], Hitonobu Tomoike[h], Kenji Sugai[c], Narihiro Minami[c,d], Hideo Kimura[d], Yu-ichi Goto[d], Hironobu Minami[i], Teruhiko Yoshida[e], Hideo Kunitoh[f], Yuichiro Ohe[f], Noboru Yamamoto[f], Tomohide Tamura[f], Nagahiro Saijo[i] and Jun-ichi Sawada[a]

Objective **CYP2C8 is known to metabolize various drugs including an anticancer drug paclitaxel. Although large interindividual differences in CYP2C8 enzymatic activity and several nonsynonymous variations were reported, neither haplotype structures nor their associations with pharmacokinetic parameters of paclitaxel were reported.**

Methods **Haplotype structures of the *CYP2C8* gene were inferred by an expectation-maximization based program using 40 genetic variations detected in 437 Japanese patients, which included cancer patients. Associations of the haplotypes and paclitaxel pharmacokinetic parameters were analyzed for 199 paclitaxel-administered cancer patients.**

Results **Relatively strong linkage disequilibriums were observed throughout the *CYP2C8* gene. We estimated 40 haplotypes without an amino-acid change and nine haplotypes with amino acid changes. The 40 haplotypes were classified into six groups based on network analysis. The patients with heterozygous **IG* group haplotypes harboring several intronic variations showed a 2.5-fold higher median area under concentration–time curve of C3′-*p*-hydroxy-paclitaxel and a 1.6-fold higher median value of C3′-*p*-hydroxy-paclitaxel/paclitaxel area under concentration–time curve ratio than patients bearing no **IG* group haplotypes ($P<0.001$ for both comparisons by Mann–Whitney *U*-test). No statistically significant differences, however, were observed between patients with and without the **IG* group (haplotypes) in clearance and area under concentration–time curve of paclitaxel, area under concentration–time curve of 6α-hydroxy-paclitaxel and 6α-, C3′-*p*-dihydroxy-paclitaxel, and area under concentration–time curve ratio of 6α-hydroxy-paclitaxel/paclitaxel.**

Conclusion ***CYP2C8*IG*** **group haplotypes were associated with increased area under concentration–time curve of C3′-*p*-hydroxy-paclitaxel and area under concentration–time curve ratio of C3′-*p*-hydroxy-paclitaxel/paclitaxel. Thus, **IG* group haplotypes might be associated with reduced CYP2C8 activity, possibly through its reduced protein levels.** ***Pharmacogenetics and Genomics*** **17:461–471 © 2007 Lippincott Williams & Wilkins.**

Pharmacogenetics and Genomics 2007, 17:461–471

Keywords: CYP2C8, haplotype, paclitaxel, pharmacokinetics

[a]National Institute of Health Sciences, [b]Tokyo Women's Medical University, [c]Musashi Hospital, [d]National Institute of Neuroscience, National Center of Neurology and Psychiatry, [e]National Cancer Center Research Institute, [f]National Cancer Center Hospital, Tokyo, [g]National Cardiovascular Center Research Institute, [h]National Cardiovascular Center, Suita and [i]National Cancer Center Hospital East, Chiba, Japan

Correspondence to Yoshiro Saito, PhD, Division of Biochemistry and Immunochemistry, National Institute of Health Sciences, 1-18-1 Kamiyoga, Setagaya-ku, Tokyo 158-8501, Japan
Tel: +81 3 5717 3831; fax: +81 3 5717 3832;
e-mail: yoshiro@nihs.go.jp

The authors, Yoshiro Saito and Noriko Katori, contributed equally to this work.

Received 11 September 2006 Accepted 21 December 2006

Introduction

Cytochrome P450s (CYPs) catalyze oxidative metabolism of a wide variety of exogenous chemicals and endogenous compounds. Human CYP2C subfamily consists of four members, CYP2C18, CYP2C19, CYP2C9, and CYP2C8, all of which are located in tandem on chromosome 10q23–24 in the order listed above [1]. CYP2C8 is a clinically important enzyme, which metabolizes various drugs such as the anticancer drug paclitaxel (PTX), the antiarrhythmic drug amiodarone, the insulin secretagogue repaglinide, the HMG-CoA reductase inhibitor cerivastatin, and the nonsteroidal antiinflammatory drug ibuprofen [1]. This enzyme is also involved in the oxidation of retinoids and fatty acids including arachidonic acid [1].

Up to 38-fold interindividual variability has been reported on PTX 6α-hydroxylation and rosiglitazone *p*-hydroxylation and *N*-desmethylation by CYP2C8 [2,3]. Effects of CYP2C8 genetic polymorphisms on metabolic activities have also been studied. Two polymorphisms first identified were 805A > T (Ile269Phe, *CYP2C8*2*) and 416G > A/1196A > G (Arg139Lys, Lys399Arg, *CYP2C8*3*). The **2* and **3* alleles were mainly found in Africans with 0.04–0.18 frequencies, and in Caucasians with 0.10–0.23 frequencies, respectively [1]. Both alleles were associated with decreased enzymatic activities for PTX 6α-hydroxylation *in vitro* [4–6]. *CYP2C8*4* allele (792C > G, Ile264Met) was found in British Caucasians [6]. We found 475delA (*CYP2C8*5*) in Japanese, and this allele leads to a frame shift at codon 159 followed by a stop codon at residue 177 [7]. We also found five additional polymorphisms (*CYP2C8*6* to **10*) in Japanese [8]. Among them, *CYP2C8*7* (556C > T, Arg186X) and **8* (556C > G, Arg186Gly) are different nucleotide variations at the same position. The former variation results in the stop codon, and the latter leads to an amino-acid substitution with a markedly reduced hydroxylation activity to PTX *in vitro*. Recently, two additional variations, *CYP2C8*13* (669T > G, Ile223Met) and **14* (712G > C, Ala238Pro), have been reported [9].

To date, a few reports have shown the impact of *CYP2C8*3* alleles on drug pharmacokinetics. The presence of **3* was associated with reduced clearance and increased area under concentration-time curve (AUC) of (*R*)-ibuprofen [10]. In contrast, significantly reduced AUC and C_{max} of repaglinide were observed in the patients with heterozygous **3* but not in patients with heterozygous **4* [11]. As for PTX, previous studies failed to show the influence of *CYP2C8* variations on PTX pharmacokinetics [12,13].

Haplotypes, linked polymorphisms on the same chromosome, often show more precise and strong association with phenotypes such as adverse reaction and/or pharmacokinetics of drugs than individual polymorphisms [14]. In this study, we determined/inferred haplotype structures of the *CYP2C8* gene using genetic polymorphisms detected in 437 Japanese patients. Then, association analysis was performed between the haplotypes and pharmacokinetic parameters for PTX and its metabolites. PTX is metabolized to form C3′-*p*-hydroxy-PTX (3′-*p*-OH-PTX) and 6α-hydroxy-PTX (6α-OH-PTX): both metabolites are further hydroxylated to 6α-,C3′-*p*-dihydroxy-PTX (diOH-PTX) [2,15,16]. CYP2C8 metabolizes PTX and 3′-*p*-OH-PTX into 6α-OH-PTX and diOH-PTX, respectively. Another enzyme, CYP3A4, metabolizes PTX and 6α-OH-PTX into 3′-*p*-OH-PTX and diOH-PTX, respectively. Previously, we showed that a *CYP3A4* haplotype affected the pharmacokinetics of these metabolites [9]. In this study, effects of *CYP2C8* haplotypes on PTX metabolism were investigated.

Materials and methods

Patients for DNA sequencing

A total of 437 Japanese patients (235 cancer patients administered PTX, 106 arrhythmic patients, and 96 epileptic patients) participated in this study. This population included 54 patients, who were previously used to identify the *CYP2C8*5* allele and four intronic variations [7], and seven patients with *CYP2C8*6* to **10* [8], **13* and **14* alleles [9]. Written informed consent was obtained from all participating patients. The ethical review boards of the National Cancer Center, the National Cardiovascular Center, the National Center of Neurology and Psychiatry, and the National Institute of Health Sciences approved this study.

Polymerase chain reaction conditions and DNA sequencing

Genomic DNA was extracted from whole blood leukocytes. First, the entire *CYP2C8* gene except for −8.8 and −1.9 kb enhancer regions was amplified in two portions (from the promoter region to exon 5, and exons 6–9) using the primer sets listed in the 'first polymerase chain reaction (PCR)' section of Table 1. Amplification was performed from 200 ng of genomic DNA using 1.25 units of Z-T (Takara Bio. Inc., Shiga, Japan) with 0.2 μmol/l of the primer sets. The first PCR conditions were 30 cycles of 98°C for 5 s, 55°C for 5 s, and 72°C for 190 s. Then, each exon (except for simultaneous amplification of exons 2 and 3) was amplified by Ex-Taq (1.25 units) with a set of primers (0.2 μmol/l) listed in the 'second PCR' section of Table 1 (primers were designed in the intronic regions or promoter region). The second-round PCR conditions were 94°C for 5 min, followed by 30 cycles of 94°C for 30 s, 60°C for 1 min, and 72°C for 2 min, and then a final extension at 72°C for 7 min. As for the −8.8 and −1.9 kb enhancer regions, amplification was performed directly from 50 ng of genomic DNA under the same conditions as in the second round PCR. Thereafter, the PCR products were treated with a PCR Product Pre-Sequencing Kit (USB Co., Cleveland, Ohio, USA) and directly sequenced on both strands using an ABI BigDye Terminator Cycle Sequencing Kit (Applied Biosystems, Foster City, California, USA) with the primers listed in the 'Sequencing' section of Table 1. For the −8.8 and −1.9 kb enhancer regions, promoter region, exon 4, and exons 7–9, the primer sets for the second PCR were also utilized for sequencing. The excess dye was removed by a DyeEx 96 kit (Qiagen, Hilden, Germany). The eluates were applied to an ABI Prism 3700 DNA Analyzer (Applied Biosystems). All detected variations were confirmed by repeating the PCR from the genomic DNA and sequencing of the newly generated PCR products. Genbank accession number NT_030059.12 was used for the reference sequence. Under conditions used, the −8.8 kb enhancer region (pregnanex receptor/constitutive androstane receptor-binding site and its surrounding region), −1.9 kb enhancer region (glucocorticoid receptor-binding site and

Table 1 Primers used for the sequencing of *CYP2C8*

	Amplified and sequenced region	Forward primer		Reverse primer		Amplified length (bp)
		Sequences (5′–3′)	Position at 5′-end[b]	Sequences (5′–3′)	Position at 5′-end[b]	
First PCR	Promoter to exon 5	CTGTGGTGTAAGTGGTAATGAAC	15578696	AAAAGCCCTGAGAACCTATAATC	15563106	15591
	Exons 6–9	TAAGTATTTGTCCCAGTGCTCTC	15562092	TAGCAACTATACAAGCACGGG	15544271	17822
Second PCR	− 8.8 kb	CCCAAAAAAGAGCAGGTGTAGCCAT	15586590	TTACTGTCTGTCAAGTGGACCTATC	15586279	312
	− 1.9 kb	CTGACCCACATTTTACTCAACTG	15579731	CCCAGTTTAGAGAGGAGAAAGTTAG	15579471	261
	Promoter	GTCCTGTTCTCCCAGAGTTTC	15578600	TCTCCAGAGTGAAAAGAGAAGC	15577623	978
	Exon 1	TCATAAATTCCCAACTGGTC	15578062	GAGCTTGCAGTGAGTGGAGA	15577279	784
	Exons 2–3	TGCTGAATGTGTTGAAGTGAGG	15576234	CTCCCTTGTCTCTGTGCTTC	15575334	901
	Exon 4	AGGCAGTGGATGTGAATAACC	15573481	TCTGTACCTAAAGATTGGAGGCTG	15572897	585
	Exon 5	TCTCAGCATACTATCACAAGGAC	15567211	TAAGGGCTATGTCAATGTGC	15566208	1004
	Exon 6	ACTAACCTAAGCAGCGAATGA	15554467	TTTTCATCTCCCCACCACAGCATT	15553696	772
	Exon 7	GGCTGGTTGTACTTCTGGAC	15551500	AATAGCAGAAAGTCCATCAAGC	15551034	467
	Exon 8	GAAGTGATGAAATAGAGCGGCAA	15547620	TAGTGGCAGAGTTCAGTCAAACC	15546922	699
	Exon 9	TGGGAATAAATAAAGAAATGACTG	15545899	GTCAGCATTAGAAAAGTATTAGCA	15545166	734
Sequencing[a]	Exon 1	CAGTGTTTCTCCATCATCACAGC	15577988	TTCAGAGGGAGTATTTTGCTTT	15577388	
	Exon 2	CATCACAGGCCATCTATAAGTGG	15576165	CCCCCTCACCCCAGTTACC	15575764	
	Exon 3	GGTAACTGGGGTGAGGGGG	15575782	CTCCCTTGTCTCTGTGCTTC	15575334	
	Exon 5	GGAACATTACACACTGGGGT	15567115	ATTATTTTTATTTCAAGAAGAGGG	15566396	
	Exon 6	ACTAACCTAAGCAGCGAATGA	15554467	TCTCTGTCATCCTCCTCCATT	15553904	

[a]Primer sets for the second PCR were used for the − 8.8 kb, − 1.9 kb, promoter, exons 4, 7, 8 and 9.
[b]The position in the reference sequence, NT_030059.12.

its surrounding region), promoter region (up to 890 bases upstream of the translational initiation site, including hepatocyte nuclear factor 4α-binding site) [17] and all nine exons and its flanking introns were successfully sequenced for all patients analyzed.

Linkage disequilibrium and haplotype analyses

Hardy–Weinberg equilibrium and linkage disequilibrium (LD) analyses were performed by SNPAlyze software (version 3.1, Dynacom Co., Yokohama, Japan), and a pairwise LD between variations was obtained for the $|D'|$ and rho square (r^2) values. Some haplotypes were unambiguously determined from patients with homozygous variations at all sites or a heterozygous variation at only one site. Separately, diplotypes (a combination of haplotypes) were inferred by LDSUPPORT software, which determines the posterior probability distribution of the diplotype configuration for each patient based on estimated haplotype frequencies [18]. Diplotypes of all patients were inferred with probabilities (certainties) of more than 0.95 except for 18 patients. Haplotypes without amino-acid changes were designated as **1*, and haplotypes with amino-acid changes were numbered according to the assignments by the Human Cytochrome P450 (CYP) Allele Nomenclature Committee (*http://www.cypalleles.ki.se/cyp2c8.htm*). The estimated haplotypes (subtypes) were tentatively shown with numbers plus small alphabetical letters. The haplotypes (subtypes) already assigned by the Committee were described as numbers plus capital alphabetical letters (**1A*, **1B*, and **1C*). Network analysis was performed using haplotypes detected in more than two patients with Network 4.1.1.2 by median-joining algorithm (*http://fluxus-engineering.com/*) [19].

Patients administered PTX and pharmacokinetic analysis

Demographic data of 235 PTX-administered cancer patients including their eligibility criteria were described previously [9]. Of the 235 patients, 199 (185 nonsmall cell lung cancer, four thymic carcinoma, four breast cancer, and six other cancers) were treated with PTX at doses of 175–210 mg/m^2 (the high-dose group in the previous paper [9]) at the National Cancer Center, and used for analysis of associations between haplotypes and pharmacokinetic parameters. These patients consisted of 139 men and 60 women with a mean age of 60.8 (range: 29–81) years. All patients were naive to PTX and pretreated with dexamethasone and an antiallergic agent (diphenhydramine or chlorpheniramine maleate) as prophylactics against hypersensitivity reactions. Carboplatin or nedaplatin was coadministered to almost all patients immediately after PTX treatment. The ethical review boards of both the National Cancer Center and the National Institute of Health Sciences approved this study. Written informed consent was obtained from all patients.

Methods for pharmacokinetic analysis were described previously, and the parameters obtained previously were used for the current association studies [9].

Statistical analysis for association studies

Differences in medians of pharmacokinetic parameters were analyzed by the Kruskal–Wallis test or the Mann–Whitney *U*-test. Statistical analysis was done using Prism v.4.00 (GraphPad Software Inc., San Diego, California, USA) and SAS v.8.2 (SAS Institute Inc., Cary,

North Carolina, USA). A significance level of 0.05 was applied to all two-tailed analyses.

Results

CYP2C8 variations

We reported previously the *CYP2C8* nonsynonymous variations, **5* (475delA, 159fsX18) [7], **6* (511G > A, Gly171Ser), **7* (556C > T, Arg186X), **8* (556C > G, Arg186Gly,) **9* (740A > G, Lys247Arg), **10* (1149G > T, Lys383Asn) [8], **13* (669T > G, Ile223Met), and **14* (712G > C, Ala238Pro) [9]. These variations were, however, very rare in the Japanese, and it was rather difficult to perform statistical evaluation on their in-vivo associations with altered function, because of low frequencies [9]. Therefore, we continued resequencing this gene including the promoter and intronic regions for up to 437 patients. The enhancer regions were also sequenced for 199 patients administered PTX. Table 2 summarizes the obtained data, where Genbank accession number NT_030059.12 was utilized for the reference sequence. Forty variations, including 11 novel ones, were detected in 437 patients. Because we did not find any significant differences in the genotype distributions among the three disease types ($P \geq 0.05$ by χ^2 test or Fisher's exact test), data from all patients were analyzed as one group. All detected variations were found in Hardy–Weinberg equilibrium ($P \geq 0.05$ by χ^2 test or Fisher's exact test), except for two polymorphisms IVS3−97delT and IVS3−21_−20insT. These deviations were due to the occurrence of one extra homozygote, and the existence of these homozygotes was confirmed by amplification of DNA by another set of primers and resequencing (data not shown). The overall frequencies of the previously reported nonsynonymous variations *CYP2C8*5*, **6*, **7*, **8*, **9*, **10*, **12* (1382_1384del TTG, del 461Val), **13*, and **14* were 0.002, 0.002, 0.001, 0.001, 0.001, 0.001, 0.001, 0.001, and 0.001, respectively, and they were all found as heterozygotes. We also detected −271C > A (*CYP2C8*1B*) and −370T > G (**1C*) at frequencies of 0.106 and 0.330, respectively. The frequency of the **1C* allele in Japanese is approximately 5.4-fold higher than in Caucasians [6]. We did not detect any variation in the functional hepatocyte nuclear factor 4α-binding site (−155 to −137 from the translational start site on NT_030059.12) [17], and its surrounding region in 437 patients. Also no variation was found in pregnanex receptor/constitutive androstane receptor-binding site (−8807 to −8788), glucocorticoid receptor-binding site (−1930 to −1910) [17], and their surrounding regions in 199 PTX-administered patients.

Linkage disequilibrium analysis

Using the 15 detected polymorphisms greater than 0.03 in frequency, LD was analyzed for $|D'|$ and r^2 values (Fig. 1). $|D'|$ values were more than 0.9 in 89 out of 105 (85%) combinations (Fig. 1, lower left). For r^2 values (Fig. 1, upper right), strong LD ($r^2 \geq 0.80$) was observed among IVS2-64A > G, IVS2−13_−12insT, IVS3−166A > G, IVS4−150G > A, IVS4−94T > C, IVS6 + 196G > A, IVS7 + 49T > A, IVS8 + 106G > A, and 1497 (*24)C > T. These polymorphisms were also moderately linked with −411T > C and −370T > G ($r^2 \geq 0.49$). Strong LD was also observed between IVS3-21T > A and IVS4 + 151G > A ($r^2 = 0.93$), and both variations were partially linked with IVS8-204A > G ($r^2 \geq 0.57$). The r^2 values of the other combinations were below 0.33. Collectively, relatively strong LDs were observed throughout the *CYP2C8* gene, suggesting that one LD block covers the entire region analyzed (approximately 33 kb). Thus, *CYP2C8* haplotypes were analyzed as one block.

Haplotype analysis

Haplotypes determined/inferred are shown in Fig. 2. The haplotypes obtained in this study were tentatively shown as a number plus small alphabetical letter except for the haplotypes already publicized on the Human Cytochrome P450 (*CYP*) Allele Nomenclature Committee website, which are described as the number plus capital alphabetical letter (**1A*, **1B*, and **1C*). Several haplotypes were first unambiguously assigned by homozygous single nucleotide polymorphisms at all sites (**1d*-**1f*, **1j*, and **1w*) or a heterozygous single nucleotide polymorphism at only one site (**1k*, **1m*, **1t*, **1z*, **1aa*, and **8b*). Separately, diplotypes for each patient were inferred by LDSUPPORT software. The additionally inferred haplotypes were 27 **1* subtypes (**1g*, **1h*, **1l*, **1n* to **1s*, **1u*, **1v*, and other very rare 17 haplotypes), and eight haplotypes with nonsynonymous variations (**5b*, **6b*, **7b*, **9b*, **10b*, **12b*, **13b*, and **14b*). The **1* subtypes inferred in only one patient are grouped into 'others' in Fig. 2, and haplotypes with nonsynonymous variations are described with '?' except for unambiguous **8b*, since the predictability for these very rare haplotypes is known to be low in some cases. Overall, 49 haplotypes were determined and/or inferred. The most frequent haplotype was **1d* (frequency: 0.366), followed by **1e* (0.289), **1f* (0.113), and **1B* (0.085). Frequencies of the other haplotypes were less than 0.05.

Next, we performed network analysis using haplotypes found in more than two patients to clarify the relationships among the haplotypes. The results showed that the **1* subtypes could be further classified into six groups, **1A*, **1B*, **1D*, **1E*, **1G*, and **1J* groups (Fig. 3). The grouping of **1* subtypes was also shown in Fig. 2. Their frequencies were 0.435 (**1E* group), 0.381 (**1D*), 0.103 (**1B*), 0.030 (**1G*), 0.021 (**1A*), and 0.013 (**1J*). Five rare unclassified **1* subtypes were shown in '**1 others*'. Haplotypes **5b* and **6b* were shown to be derived from **1d* and **1B*, respectively.

Effects of *CYP2C8* haplotypes on PTX metabolism

CYP2C8 catalyzes biotransformation of PTX into 6α-OH-PTX and of 3′-*p*-OH-PTX into diOH-PTX. The effects of *CYP2C8* haplotypes on PTX clearance, AUCs of PTX

Table 2 Summary of *CYP2C8* variations detected in a Japanese population

SNP ID					Position					Number of subjects			
This study	NCBI (dbSNP)	JSNP	Reference	Location	NT_030059.12	From the translational initiation site or from the nearest exon	Nucleotide change and flanking sequences (5′ to 3′)	Amino acid change	Allele name	Wild-type	Hetero-zygotes	Homo-zygotes	Frequency
MPJ6_2C8029[a]				5′-flanking	15578352_15578350	−667_−665[b]	ATAATGTAATAA**TAA**/-CACAAATATTAT			435	2	0	0.002
MPJ6_2C8030	rs7912549		[4]	5′-flanking	15578096	−411[b]	ACATTTTTTATA**T/C**ACAAAATATAGA			152	218	67	0.403
MPJ6_2C8031	rs17110453		[6]	5′-flanking	15578055	−370[b]	CAAGGTCATAAAT**/G**TCCCAACTGGTC		*1C*	201	184	52	0.330
MPJ6_2C8023	rs7909236		[6]	5′-flanking	15577956	−271[b]	AGCACATTGGAA**C/A**AACCAGGGACTT		*1B*	352	77	8	0.106
MPJ6_2C8032[a]				Intron 1	15576171	IVS1−197	CTGGGTCATTGC**G/A**TGGCACATCACA			436	1	0	0.001
MPJ6_2C8014			[7]	Intron 1	15576095	IVS1−121	ATTCAGAAATAT**C/T**GAATCTATGTGT			436	1	0	0.001
MPJ6_2C8010	rs2275622	IMS-JST071855	[4]	Intron 2	15575704	IVS2−64	TGCATGGCTGCC**A/G**AGTGTTGCAGCA			120	212	105	0.483
MPJ6_2C8001	rs11572078	IMS-JST077576	[4]	Intron 2	15575653_15575652	IVS2−13_−12	AGTTTCTGCCCC**-/T**TTTTTTTATTAG			142	205	90	0.441
MPJ6_2C8015			[7]	Exon 3	15575497	475[b]	GAGTTGAGAAAAA**/-**CCAAGGGTGGGT	159fsX18	*5*	435	2	0	0.002
MPJ6_2C8019	rs3752988	IMS-JST105874		Intron 3	15573409	IVS3−166	AACTCATATTTA**A/G**GGTAAAAGTAAT			141	207	89	0.441
MPJ6_2C8016	rs11572091		[7]	Intron 3	15573340	IVS3−97	TTTGTAAGATATT**/-**GTTTAAAATTTC			427	9	1	0.013
MPJ6_2C8033[a]				Intron 3	15573264_15573263	IVS3−21_−20	AATAATTTTTTT**-/T**AAAAATTTTTAA			436	0	1	0.002
MPJ6_2C8004	rs7098376		[5]	Intron 3	15573264	IVS3−21	TAATAATTTTTTT**/A**AAAAATTTTTAA			409	28	0	0.032
MPJ6_2C8034			[8]	Exon 4	15573214	511[b]	ACTTTCATCCTG**G/A**GCTGTGCTCCCT	Gly171Ser	*6*	435	2	0	0.002
MPJ6_2C8035			[8]	Exon 4	15573169	556[b]	GTTTTCCAGAAA**C/T**GATTTGATTATA	Arg186X	*7*	436	1	0	0.001
MPJ6_2C8036			[8]	Exon 4	15573169	556[b]	GTTTTCCAGAAA**C/G**GATTTGATTATA	Arg186Gly	*8*	436	1	0	0.001
MPJ6_2C8037[a]				Intron 4	15573039	IVS4+44	CATTTATTCAAG**G/T**TTGTAGGGAAGA			436	1	0	0.001
MPJ6_2C8024	rs11572093		[4]	Intron 4	15572932	IVS4+151	CTTTGATTTCCT**G/A**TTCAAAATTTTC			411	26	0	0.030
MPJ6_2C8038[a]				Intron 4	15567024	IVS4−230	GACGAGTTATTG**G/A**GTGCAGTACACC			436	1	0	0.001
MPJ6_2C8039[a]				Intron 4	15567008	IVS4−214	CAGTACACCAAC**C/A**TGGCACATGTAT			436	1	0	0.001
MPJ6_2C8020	rs1926705			Intron 4	15566944	IVS4−150	AGAACTTAAAGT**G/A**TAATAAAAAATG			119	214	104	0.483
MPJ6_2C8025[a]				Intron 4	15566937	IVS4−143	AAAGTGTAATAA**A/G**AAATGTATATAT			436	1	0	0.001
MPJ6_2C8012	rs11572101			Intron 4	15566888	IVS4−94	GACATGATGTCTT**/C**ATTCATATTTAT			141	207	89	0.441
MPJ6_2C8040			[9]	Exon 5	15566768	669[b]	CCCTCTACTCATT**/G**GATTGTTTCCCA	Ile223Met	*13*	436	1	0	0.001
MPJ6_2C8041			[9]	Exon 5	15566725	712[b]	CTTAAAAATGTT**G/C**CTCTTACACGAA	Ala238Pro	*14*	436	1	0	0.001
MPJ6_2C8026			[8]	Exon 5	15566697	740[b]	ACATTAGGGAGAA**/G**AGTAAAAGAACA	Lys247Arg	*9*	436	1	0	0.001
MPJ6_2C8027[a]				Intron 5	15566597	IVS5+21	TTAGCAACAGAT**C/T**AGTATTTTGATT			435	2	0	0.002
MPJ6_2C8042[a]				Intron 6	15553909	IVS6+184	GGAGGAGGATGA**C/G**AGAGATCAGTAG			433	4	0	0.005
MPJ6_2C8021	rs1891071	IMS-JST082397		Intron 6	15553897	IVS6+196	CAGAGATCAGTA**G/A**AAACAGTATGGC			124	215	98	0.470
MPJ6_2C8043[a]				Intron 6	15553794	IVS6+299	ATTGCCCTAGTA**T/C**TGAATGTTGGTT			436	1	0	0.001
MPJ6_2C8044			[8]	Exon 7	15551173	1149[b]	CCTCATCCCCAA**G/T**GTAAGCTTGTTT	Lys383Asn	*10*	436	1	0	0.001
MPJ6_2C8013	rs2275620	IMS-JST071852	[4]	Intron 7	15551124	IVS7+49	CTGAAATTTCCA**T/A**AGTGCTGGTTTG			124	215	98	0.470
MPJ6_2C8017			[7]	Intron 7	15551102	IVS7+71	TTGGTTCCAACC**C/T**TCTAACAACACA			430	7	0	0.008
MPJ6_2C8007			[5]	Exon 8	15547241	1230[b]	CTTTGACCCTGG**C/T**CACTTTCTAGAT	Gly410Gly		424	13	0	0.015
MPJ6_2C8008	rs1934951	IMS-JST071853	[5]	Intron 8	15547074	IVS8+106	GAATTGCTATTT**G/A**TCCATGATCAAG			143	201	93	0.443
MPJ6_2C8022	rs2275621	IMS-JST071854		Intron 8	15547050	IVS8+130	GAGCACCACTCTT**/C**AACACCCATGTG			430	7	0	0.008
MPJ6_2C8018	rs11572177		[7]	Intron 8	15545796	IVS8−204	GATAGCAAATATA**/G**TCTCTTTTGTA			403	33	1	0.040
MPJ6_2C8045	rs3832694	IMS-JST091412		Exon 9	15545502_15545500	1382_1384[b]	ACCTGAAATCTG**TTG/-**ATGATTTAAAGA	del 461Val	*12*	436	1	0	0.001
MPJ6_2C8009	rs1058932	IMS-JST091413	[5]	3′-UTR	15545387	1497[b](*24)[c]	CCATCTGGCTGC**C/T**GATCTGCTATCA			143	196	98	0.449
MPJ6_2C8046[a]				3′-UTR	15545208	1676[b](*203)[c]	ACTCTGTAACAC**T/-**TGTATTAATTGC			434	3	0	0.003

[a]Novel variations detected in our study.
[b]A of the translation initiation codon ATG is numbered +1.
[c]The nucleotide number from the end of translational termination codon.
SNP, single nucleotide polymorphism.

Fig. 1

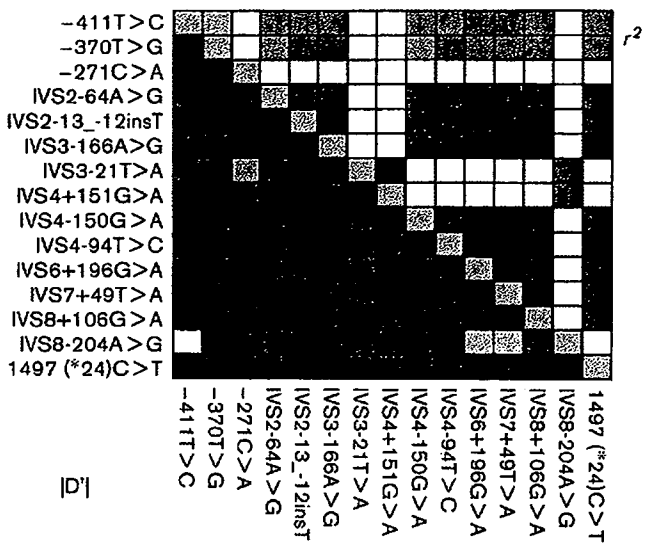

Linkage disequilibrium (LD) analysis of *CYP2C8*. Pairwise LD between variations with ≥ 3% frequencies is expressed as $|D'|$ (lower left) and r^2 (upper right) by 10-graded blue colors. A denser color represents a higher linkage.

and its metabolites, and metabolic ratios (ratios of metabolite AUCs to PTX AUC) were investigated in 199 PTX-administered patients.

Because nonsynonymous variations were all rare, we focused on the effects of diplotypes using grouped **1* haplotypes (i.e. **1A*, **1B*, etc). No significant differences were observed in clearance of PTX, AUCs of PTX, 6α-OH-PTX and diOH-PTX, and AUC ratio of 6α-OH-PTX/PTX among the grouped **1*-diplotypes found in more than three patients (data not shown). A statistically significant deviation, however, was observed in AUC of 3′-*p*-OH-PTX among the grouped **1*-diplotypes ($n \geq 3$) ($P = 0.014$ by Kruskal–Wallis test) (Fig. 4a). Furthermore, AUC ratio of 3′-*p*-OH-PTX/PTX also showed a tendency to be different among the grouped **1*-diplotypes of $n \geq 3$ by the same test ($P = 0.071$) (Fig. 4b). Careful analysis revealed that significant differences in both parameters were observed between **1D/*1D* and **1G/*1D* patients ($P < 0.05$ for both parameters, Mann–Whitney *U*-test) and between **1E/*1E* and **1G/*1E* patients ($P < 0.001$ for AUC of 3′-*p*-OH-PTX and $P < 0.01$ for AUC ratio of 3′-*p*-OH-PTX/PTX) (Fig. 4).

Next, heterozygous **1G* diplotypes were combined into **1G/non-*1G* diplotypes ($n = 11$). Because no significant differences were observed among the other **1/*1* groups, all the other **1/*1* diplotypes were combined into one group, designated as *non-*1G/non-*1G*. As shown in Fig. 5a, the median AUC of 3′-*p*-OH-PTX was about 2.5-fold higher in the **1G/non-*1G* patients than in the *non-*1G/non-*1G* patients ($P < 0.001$ by Mann–Whitney *U*-test). The median value of 3′-*p*-OH-PTX/PTX AUC ratio was also about 64% higher in the **1G/non-*1G* patients than in the *non-*1G/non-*1G* patients ($P < 0.001$, Fig. 5b). In contrast, there were no significant differences in AUC of 6α-OH-PTX and AUC ratio of 6α-OH-PTX/PTX between the two groups (Fig. 5c and d) although the AUC ratio was about 9% lower in the **1G/non-*1G* patients than in the *non-*1G/non-*1G* patients (Fig. 5d). Considering the metabolic route of PTX, these findings suggest that CYP2C8 activity is probably reduced in the **1G*-bearing patients.

Recently, we have shown that *CYP3A4*16B* (and probably **6*, $n = 1$) decreases the AUC ratio of 3′-*p*-OH-PTX/PTX, and that no other major *CYP3A4* haplotypes significantly affect the AUC ratio and other PK parameters analyzed [9]. Therefore, we analyzed the effects of **1G* on the AUC of 3′-*p*-OH-PTX and AUC ratio of 3′-*p*-OH-PTX/PTX excluding *CYP3A4*16B*- and **6*-bearing patients and confirmed the increasing effects of **1G* ($P < 0.001$ for both by Mann–Whitney *U*-test). In addition, the significantly increasing effects of *CYP2C8*1G* were also observed within *CYP3A4*1A/*1A* patients ($P < 0.001$ for AUC of 3′-*p*-OH-PTX and $P < 0.01$ for AUC ratio of 3′-*p*-OH-PTX/PTX, Mann–Whitney *U*-test). Furthermore, distributions of *CYP3A4* diplotypes/haplotypes were not significantly different between the *CYP2C8*1G/non-*1G* patients and the *non-*1G/non-*1G* patients ($P > 0.05$ by Fisher's exact test). These results suggest that the effects of *CYP2C8*1G* are independent of the *CYP3A4* genotypes. Gender also affects the AUC ratio of 3′-*p*-OH-PTX/PTX [9]. Statistical analysis using data from men only also gave almost the same increasing effects of **1G* ($P < 0.001$ for the AUC of 3′-*p*-OH-PTX and $P = 0.001$ for the AUC ratio of 3′-*p*-OH-PTX/PTX, Mann–Whitney *U*-test).

To identify further the genetic variation responsible for the increased AUC of 3′-*p*-OH-PTX and increased AUC ratio of 3′-*p*-OH-PTX/PTX, we next focused on the variations in the **1G* group. Among them, the patients bearing IVS3-21T > A showed statistically significant increases in these parameters compared with the patients without this variation ($P < 0.001$ for both parameters, Mann–Whitney *U*-test). The **1t* haplotype also harbored IVS3−21T > A, and one patient with the **1t/*1d* diplotype (grouped into **1D/*1D*) had the second highest AUC of 3′-*p*-OH-PTX (1.07 h*μg/ml) and the second highest AUC ratio of 3′-*p*-OH-PTX/PTX (0.0497) in the 24 **1D/*1D* patients (Fig. 4, grey arrowheads). These findings suggest that IVS3−21T > A might be involved in the altered CYP2C8 activity, although we cannot exclude the possibility that other identified/unidentified linked variation is causative.

Fig. 2

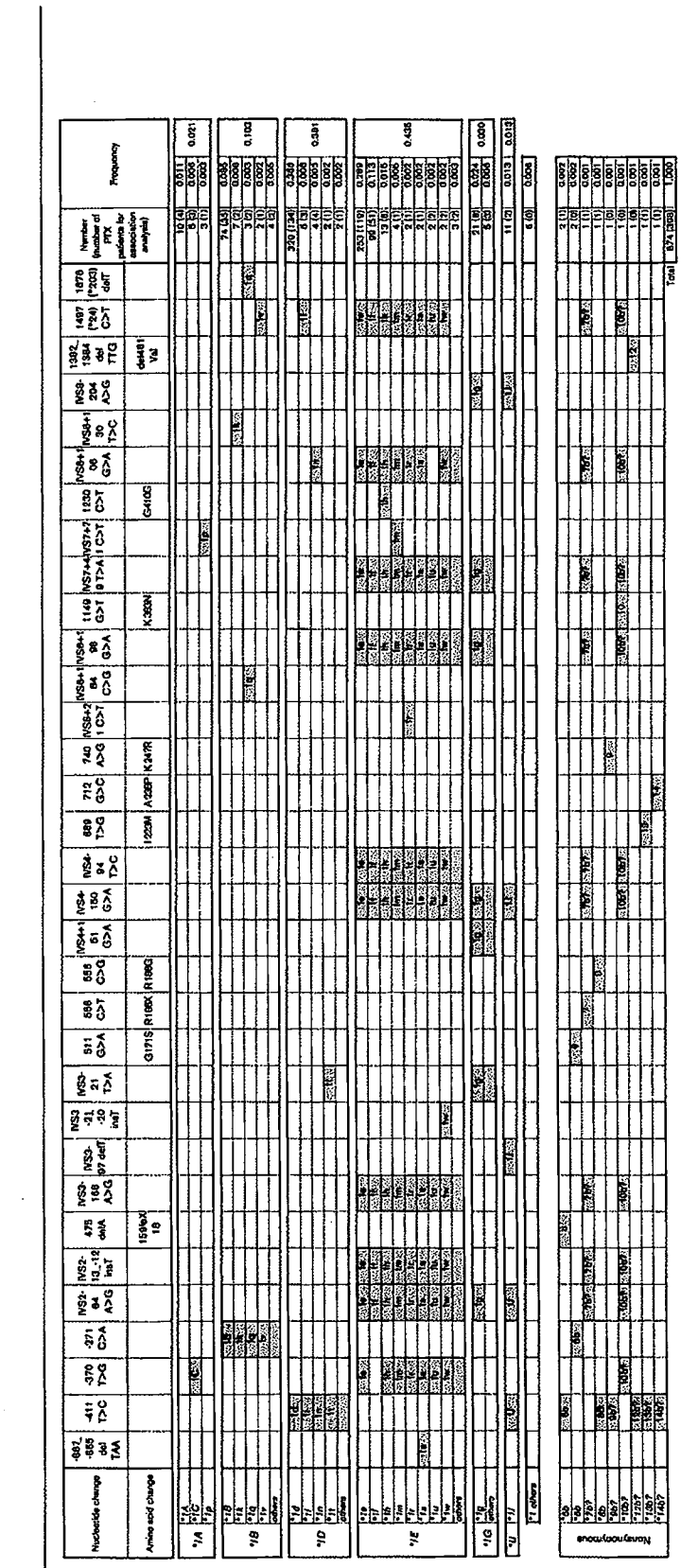

Haplotype structures of *CYP2C8* in Japanese population. Haplotypes are described with numbers plus alphabetical letters, and the **1* haplotypes (without amino-acid change) were grouped based on network analysis (Fig. 3). Because rare **1* haplotypes found in only one individual were grouped into 'others', the seven variations detected only in the rare haplotypes (IVS1 − 197G>A, IVS1 −121C>T, IVS4+44G>T, IVS4 − 230G>A, IVS4 − 214C>A, IVS4 − 143A>G, and IVS6+299T>C) are not shown in this figure. Numbers in parenthesis in the 'Number' section indicate patient numbers used for association analysis for pharmacokinetic parameters of PTX. White, major allele; yellow with a haplotype name, minor allele; yellow without a haplotype name in 'others;' common variations of the 'others' group. In yellow with a haplotype name, nonsynonymous variations are shown by a red number.

Fig. 3

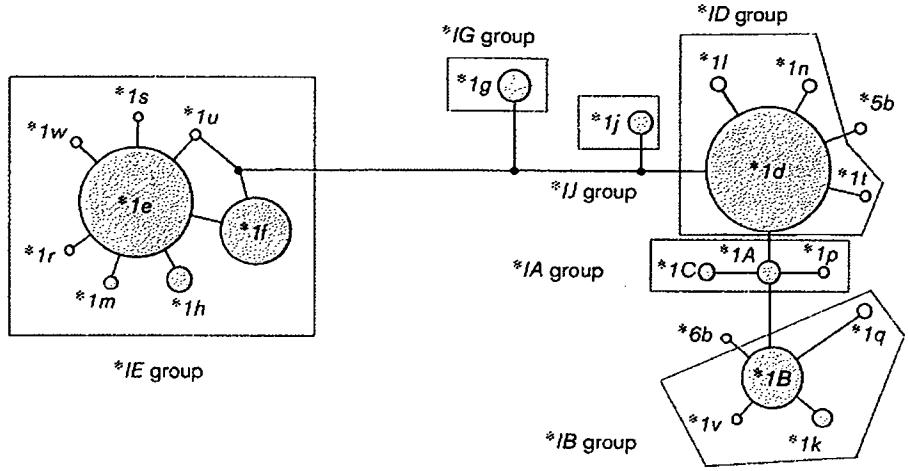

Network analysis of *CYP2C8* haplotypes. Haplotypes found in at least two patients are shown. The areas of each circle represent the approximate frequency of each haplotype. The **1* subgroups are enclosed by red lines.

Discussion

All nonsynonymous variations of *CYP2C8* found in Japanese were rare (frequencies ≤ 0.002), and thus we could not apply statistical analysis for their associations with pharmacokinetic parameters of PTX [9]. As shown in Fig. 4b, the AUC ratio of 3′-*p*-OH-PTX/PTX of a patient with heterozygous **5b* haplotype (with 475delA, 159fsX18, no activity) was, however, the third highest (2.8-fold higher than median value) in all 199 patients analyzed. In addition, the patient with heterozygous **7b* (with 556C > T, Arg186X, no activity) had the lowest AUC ratio of 6α-OH-PTX/PTX (approximately one-fifth of the median value) (data not shown). Thus, at least some of the nonsynonymous *CYP2C8* variations described in this paper probably affect the PTX metabolism *in vivo*. These rare variations, however, cannot fully explain the interindividual differences in the CYP2C8 activity. Therefore, we focused on the **1* haplotypes without amino-acid change. The estimated *CYP2C8 *1* haplotypes could be classified into six haplotype groups (**1A*, **1B*, **1D*, **1E*, **1G*, and **1J*) based on network analysis, and their effects on PTX metabolism were analyzed.

This study revealed that the AUC of 3′-*p*-OH-PTX and AUC ratio of 3′-*p*-OH-PTX/PTX were increased in the **1G*-bearing patients. It must be noted that AUC of 3′-*p*-OH-PTX was considerably increased (2.5-fold). The 3′-*p*-OH-PTX is generated from PTX by CYP3A4 and metabolized into diOH-PTX by CYP2C8. Thus, both CYP2C8 and CYP3A4 activities can influence the AUC of 3′-*p*-OH-PTX. In the previous study [9], we have shown that the *CYP3A4*16B* haplotype harboring 554C > G (Thr185Ser), but not the other haplotypes, increases the AUC ratio of 6α-OH-PTX/PTX and decreases the AUC ratio of 3′-*p*-OH-PTX/PTX with statistical significance. In addition, gender difference was also shown to affect both AUC ratios [9].The association of *CYP2C8*1G* group haplotypes with increased AUC of 3′-*p*-OH-PTX and AUC ratio of 3′-*p*-OH-PTX/PTX, however, could not be explained by the influence of *CYP3A4*16B* (and theoretically null haplotype **6*) or gender difference since the same conclusions were obtained even if patients with *CYP3A4*16B* and **6*, or females were excluded. Moreover, statistical analysis using data only from *CYP3A4*1A/*1A* patients also gave almost the same effects of **1G* on the AUC of 3′-*p*-OH-PTX and the AUC ratio of 3′-*p*-OH-PTX/PTX, suggesting that the effects of *CYP2C8*1G* are independent of the *CYP3A4* genotypes or gender difference. Thus, the increased AUC of 3′-*p*-OH-PTX and AUC ratio of 3′-*p*-OH-PTX/PTX can be attributed to *CYP2C8*1G*, suggesting reduced CYP2C8 activity in patients with **1G*. Moreover, transporters such as P-glycoprotein encoded by the *ABCB1* gene could contribute to the AUCs of PTX and its metabolites [20]. We reported previously that AUC of 3′-*p*-OH-PTX was slightly increased in the patients bearing **2* haplotype in block 2 of *ABCB1* (1236C > T, 2677G > T, and 3435C > T) [9]. When the frequencies of the **2* haplotype were compared between the *CYP2C8*1G/non-*1G* patients and the *non-*1G/non-*1G* patients, however, no statistically significant difference was observed ($P = 0.705$ by χ^2 test).

*CYP2C8*1G* group haplotypes harbors several variations, which are all located in introns. Thus, the mechanism for the increased AUC of 3′-*p*-OH-PTX and AUC ratio of 3′-*p*-OH-PTX/PTX is not caused by an amino-acid change. Among the variations in the **1G* group, IVS3−21T > A